

การศึกษารอบแบบข้อดีของนํ้าร้อนเหล็กกล้า ST52-3 ที่พอกผิวแข็งด้วยลวดเชื่อมหุ้มฟลักซ์  
โครเมียมสูงที่ผสมโมลิบดีนัมด้วย SMAW

นายณัฐ ตรงจิตต์รักษา

วิทยานิพนธ์นี้เป็นส่วนหนึ่งของการศึกษาตามหลักสูตรปริญญาวิศวกรรมศาสตรมหาบัณฑิต

สาขาวิชาวิศวกรรมโลหการและวัสดุ ภาควิชาวิศวกรรมโลหการ

คณะวิศวกรรมศาสตร์ จุฬาลงกรณ์มหาวิทยาลัย

ปีการศึกษา 2556

ลิขสิทธิ์ของจุฬาลงกรณ์มหาวิทยาลัย

บทคัดย่อและแฟ้มข้อมูลฉบับเต็มของวิทยานิพนธ์ตั้งแต่ปีการศึกษา 2554 ที่ให้บริการในคลังปัญญาจุฬาฯ (CUIR)

เป็นแฟ้มข้อมูลของนิสิตเจ้าของวิทยานิพนธ์ที่ส่งผ่านทางบัณฑิตวิทยาลัย

The abstract and full text of theses from the academic year 2011 in Chulalongkorn University Intellectual Repository (CUIR) are the thesis authors' files submitted through the Graduate School.

ABRASIVE WEAR OF HARDFACED ST52-3 STEEL HAMMER PARTS USING Mo-  
ALLOYED HIGH CHROMIUM ELECTRODES BY SMAW

Mr. Nut Thongchitruksa

A Thesis Submitted in Partial Fulfillment of the Requirements  
for the Degree of Master of Metallurgical and Materials Engineering Program in Engineering

Department of Metallurgical Engineering

Faculty of Engineering

Chulalongkorn University

Academic Year 2013

Copyright of Chulalongkorn University



ณัฐ ตรงจิตต์รักษา : การสึกหรอแบบขัดสีของหมอนเหล็กกล้า ST52-3 ที่พอกผิวแข็งด้วยลวดเชื่อม  
 หุ้มฟลักซ์โครเมียมสูงที่ผสม โมลิบดีนัมด้วย SMAW (ABRASIVE WEAR OF HARD FACED  
 ST52-3 STEEL HAMMER PARTS USING Mo-ALLOYED HIGH CHROMIUM  
 ELECTRODES BY SMAW) อ.ที่ปรึกษาวิทยานิพนธ์หลัก : รศ.ดร.กอบบุญ หล่อ ทองคำ, อ.ที่  
 ปรึกษาวิทยานิพนธ์ร่วม : PROF. FRITZ HARTUNG, Dr.-Ing. 66 หน้า.

งานวิจัยนี้ศึกษาผลของ โมลิบดีนัมต่อความต้านทานการสึกหรอแบบขัดสีของเหล็กกล้า  
 St52-3 ที่พอกผิวแข็งด้วยโครเมียม 20-23% โดยน้ำหนัก และไน โอเบียม 7-8% โดยน้ำหนักด้วย  
 วิธีการเชื่อมอาร์คไฟฟ้า การศึกษานี้ใช้ฟลักซ์ที่หุ้มบนลวดเชื่อมพอกผิวแข็ง 4 ชนิดที่ประกอบด้วย  
 ปริมาณของโครเมียมและไน โอเบียมตามกำหนดแต่มีปริมาณ โมลิบดีนัมแตกต่างกัน ตรวจสอบ  
 โครงสร้างจุลภาค วัดความแข็งจุลภาค และความต้านทานการสึกหรอแบบขัดสีตาม มาตรฐาน  
 ทดสอบ ASTM G65 วิธีการ D ของผิวพอกแข็ง ผลการทดลองพบว่า โครงสร้างจุลภาคดั้งเดิม  
 ประกอบด้วย คาร์ไบด์ปฐมภูมิและยูเทคติกคาร์ไบด์ โมลิบดีนัมเปลี่ยนแปลงรูปร่างของคาร์ไบด์  
 ปฐมภูมิโดยลดขนาดของคาร์ไบด์ปฐมภูมิเมื่อพื้นผิวพอกแข็งมีปริมาณ โมลิบดีนัมถึง 6.43% โดย  
 น้ำหนักซึ่งมีค่าความต้านทานการสึกหรอแบบขัดสีและค่าความแข็งจุลภาคสูงสุด การผสม  
 โมลิบดีนัมทำให้ขนาดของคาร์ไบด์ปฐมภูมิลดลงอาจเป็นเพราะว่า โมลิบดีนัมเพิ่มจุดนิวเคลียสของ  
 คาร์ไบด์ นอกจากนี้พบโครงสร้างแบบตาข่ายเมื่อปริมาณ โมลิบดีนัมในผิวพอกแข็งมีค่า 10.19%  
 โดยน้ำหนัก กลไกการเกิดการสึกหรอคือการตัดผิวระดับจุลภาคและการหลุดร่อนของคาร์ไบด์

ภาควิชา.....วิศวกรรมโลหการ.....ลายมือชื่อ.....  
 สาขาวิชา.....วิศวกรรมโลหการและวัสดุ.....ลายมือชื่อ อ.ที่ปรึกษาวิทยานิพนธ์หลัก.....  
 ปีการศึกษา.....2556.....ลายมือชื่อ อ.ที่ปรึกษาวิทยานิพนธ์ร่วม.....

## 5470187021: MAJOR METALLURGICAL ENGINEERING

KEYWORDS: HARDFACING ELECTRODE / ABRASIVE WEAR / MOLYBDENUM /  
GRAIN REFINING

NUT THONGCHITRUGSA: ABRASIVE WEAR OF HARDFACED ST52-3 STEEL  
HAMMER PARTS USING Mo-ALLOYED HIGH CHROMIUM ELECTRODES BY  
SMAW. ADVISOR: ASSOC. PROF. GOBBOON LOTHONHKUM, Dr.-Ing., CO-  
ADVISOR: PROF. FRITZ HARTUNG, Dr.-Ing., 66 pp.

This work studied the effect of Mo on abrasive wear resistance of (20-23)Cr-(7-8)Nb hardfaced St52-3 steel by shielded metal arc welding (SMAW). Four fluxes which compose of the fixed Cr and Nb but different Mo contents, coated on electrode were used. Microstructure, microhardness, and abrasive wear resistance test, following ASTM G65 procedure D, of the hardfaced surface were investigated. Primary coarse carbide and eutectic carbide are the main microstructure. Mo affects morphology of primary carbide by decreasing size. When Mo content of the hardfaced surface was up to 6.43 wt-%, the highest abrasive wear resistance and the highest microhardness were obtained. The decrease of primary carbide size by Mo addition is probably due to the increase of carbide nucleation. The network structure was also observed when the Mo content of the hardfacing surface reaches to 10.19 wt-%. The main wear mechanisms are microcutting and carbide pulling out.

Department: Metallurgical Engineering..... Student's Signature.....

Field of Study: Metallurgical and Materials Engineering.. Advisor's Signature.....

Academic Year : 2013..... Co-advisor's Signature.....

## ACKNOWLEDGEMENTS

I would like to express my thank to my advisor, Assoc. Prof. Dr. Gobboon Lothongkum and co-advisor, Prof. Dr. Fritz Hartung, for fully support not only knowledge but also inspiration. Thank go also to Assist. Prof. Dr.Sittichai Wirojanupatump and Mr.Man Tuiprae at Chiang Mai University for using abrasive wear testing machine.

The Graduate School of Chulalongkorn University for the H.M. the King's 72nd Birthday Scholarship is acknowledged. The financial and technical support by the Norton Interweld Company Limited and the electrode preparing by Zika Industries Company Limited were also acknowledged.

I would like to thank you the thesis committee, Assoc. Prof. Dr. Prasonk Sricharoenchai, Asst. Prof. Dr. Tachai Luangvaranunt, and Dr. Ekkarut Viyanit for their devoted times.

Finally, I would like to thank my mom, dad, and sister for supporting me in everything.

## CONTENTS

	Page
ABSTRACT IN THAI.....	iv
ABSTRACT IN ENGLISH.....	v
ACKNOWLEDGEMENTS.....	vi
CONTENTS.....	vii
LIST OF TABLES.....	x
LIST OF FIGURES.....	xi
LIST OF ABBREVIATIONS.....	xiv
CHAPTER I INTRODUCTION.....	1
1.1 Motivation.....	1
1.2 Objectives.....	2
1.3 Conceptual Framework.....	2
1.4 Research Hypothesis.....	3
CHAPTER II LITERATURE REVIEW.....	4
2.1 Molybdenum.....	4
2.2 Abrasive wear.....	5
2.2.1 Cutting or Scratching.....	6
2.2.2 Fracture.....	6
2.2.3 Fatigue.....	6
2.2.4 Grain pull-out.....	7

	Page
2.3 Shredders Hammer.....	7
2.4 Shield metal arc welding.....	9
2.5 Hardfacing.....	11
2.5.1 Preheating.....	11
2.5.2 Dilution.....	12
2.5.3 Relief checking.....	12
2.6 Strengthening.....	13
2.6.1 Solid solution strengthening.....	13
2.6.2 Precipitation strengthening.....	13
2.7 Testing machine.....	14
2.7.1 Abrasive wear testing.....	14
2.7.2 Microstructure analysis.....	15
2.8 Relevant research.....	16
CHAPTER III METHODOLOGY.....	33
3.1 Materials.....	33
3.2 Experimental procedure.....	34
3.3 Analysis experiment result.....	41
CHAPTER IV RESULTS.....	44
4.1 Microstructure analysis.....	44



	Page
4.2 Microhardness and abrasive wear resistance.....	56
CHAPTER V CONCLUSION AND RECOMMENDATIONS.....	60
5.1 General conclusion.....	60
5.2 Recommendations.....	60
REFERENCES.....	61
BIOGRAPHY.....	66

## LIST OF TABLES

		Page
Table 2.1	Properties of molybdenum.....	4
Table 2.2	Characteristics of alloy carbides usually found.....	13
Table 2.3	Hardness of deposit materials.....	18
Table 2.4	General results from dry wheel ASTM G65.....	18
Table 2.5	Composition (wt-%) of hardfacing electrode.....	19
Table 2.6	Chemical composition design of experimental materials.....	25
Table 2.7	Average grain size of experimental cermets.....	25
Table 2.8	Nominal compositions of Co–Cr–W–C and Co–Cr–Mo–C Stellite alloys.....	29
Table 3.1	Chemical composition of ST52-3 DIN17100 steel by emission spectrometer.....	33
Table 3.2	Chemical composition of hardfacing electrode samples as designed.....	33
Table 3.3	Abrasive wear resistance test conditions .....	37
Table 4.1	Chemical composition of hardfacing surface samples by emission spectrometer.....	45
Table 4.2	Phases for different samples from XRD patterns.....	52

## LIST OF FIGURES

		Page
Figure 2.1	Type of abrasive wear.....	6
Figure 2.2	Position of shredder hammer.....	7
Figure 2.3	Shredder hammer.....	8
Figure 2.4	Shredder hammer after use 18 days.....	9
Figure 2.5	Shield metal arc welding process.....	10
Figure 2.6	Shield metal arc welding circuit.....	10
Figure 2.7	Dilution in welding seam.....	12
Figure 2.8	ASTM G65 testing machine.....	14
Figure 2.9	Optical microscope.....	15
Figure 2.10	Hardfacing microstructure.....	17
Figure 2.11	Relation between hardness and abrasion resistance.....	19
Figure 2.12	SEM morphology of the S4 hardfacing layer.....	21
Figure 2.13	X-ray diffraction spectrum of hardfacing layer.....	22
Figure 2.14	TEM image of the hardfacing layer.....	23
Figure 2.15	Effect of the amount of Fe-Mo on wear volume loss.....	24
Figure 2.16	Effect of the amount of Fe-Mo on macrohardness and volume fraction of carbides.....	24
Figure 2.17	SEM-BSE micrographs of microstructure with different molybdenum content(wt-%).....	26
Figure 2.18	The effect of Mo content on rupture strength.....	27
Figure 2.19	The effect on Mo content on hardness.....	28
Figure 2.20	The effect on Mo content on fracture toughness.....	28
Figure 2.21	Low-stress abrasive and high-stress abrasive-wear resistance.....	30
Figure 2.22	SEM images of the scratches made above the critical load. Scratch direction was from left to right.....	31
Figure 2.23	Cracking resistance in terms of critical plastic shear strain.....	32

	Page
Figure 3.1	Schematic diagram of hardfaced samples..... 34
Figure 3.2	Base material after full hardfacing on the surface..... 35
Figure 3.3	Flat surface of hardfaced samples after grinding..... 35
Figure 3.4	Weighing scale four decimal points (Mettler Toledo AB304-S)..... 36
Figure 3.5	ASTM G65 abrasive wear dry sand-rubber wheel testing machine..... 37
Figure 3.6	Wire cutting machine (Troop TP-25)..... 38
Figure 3.7	Cross-section of hardfaced sample..... 38
Figure 3.8	Scanning electron microscope with EDX (Jeol-5800LV)..... 39
Figure 3.9	Electron probe micro analyzer (Jeol JXA-8100)..... 40
Figure 3.9	Vickers microhardness measurement machine..... 40
Figure 3.10	X-ray diffraction (XRD) machine (Bruker D8advance)..... 41
Figure 3.11	Measuring length of diamond pyramid cavity on microstructure..... 42
Figure 3.12	ASTM E562 standard test method for determining volume fraction by systematic manual point count using 100 points..... 43
Figure 4.1	Cross-section of sample after hardfacing..... 44
Figure 4.2	Porosity on hardfacing surface of sample S4..... 45
Figure 4.3	Microstructure of the top layer of samples observed by OM..... 46
Figure 4.4	Microstructure of the top surface of samples obtained by SEM..... 47
Figure 4.5	Ternary phase diagram of Fe-Cr-C system..... 48
Figure 4.6	EDX spectra of different position on the microstructure of samples..... 50
Figure 4.7	XRD patterns of hardfacing samples..... 51
Figure 4.8	Volume fraction of primary and eutectic carbides with respect to the molybdenum contents..... 53
Figure 4.9	Microstructure of different layer of sample S3..... 54
Figure 4.10	Volume fraction of total carbides in each layer of sample S3..... 55

	Page
Figure 4.11 Element composition in different layers of sample S3.....	56
Figure 4.12 Microhardness, volume loss and abrasive wear resistance of samples with different molybdenum contents.....	58
Figure 4.13 Worn surfaces of samples.....	59

**LIST OF ABBREVIATIONS**

wt-%	Percent weight total
°C	Celsius
µm	Micrometer
A	Ampere
Å	Angstrom
C	Carbon
cm.	Centimeter
Co	Cobalt
Cr	Chromium
DCEP	Direct current electrode positive
EDX	Energy dispersive X-ray spectroscopy
EPMA	Electron probe micro analyzer
FCAW	Flux cored arc welding
Fe	Ferrous
g	gram
GPa	Gigapascals
HRA	Rockwell hardness scale A
HRC	Rockwell hardness scale C
HV	Vickers hardness

K	Kelvin
kgf.	Kilogram force
M	Metal
m	Meter
MAG	Metal active gas
MIG	Metal inert gas
min.	Minute
mm.	Millimeter
Mn	Manganese
Mo	Molybdenum
MPa	Megapascals
N(element)	Nitrogen
N(force)	Newton
Nb	Niobium
OM	Optical microscope
P	Phosphorus
rpm	Revolution per minute
S	Sulfur
SAW	Submerged arc welding
SEM	Scanning electron microscope
Si	Silicon

SMAW	Shielded metal arc welding
Ti	Titanium
TIG	Tungsten inert gas
V	Vanadium
V	Voltages
W	Tungsten
W	Watts
XRD	X-ray Diffraction



## CHAPTER I

### INTRODUCTION

#### 1.1 Motivation

Hardfacing is a metallurgical process. The tougher or harder metal is coated on the surface of the softer base metal by various welding processes such as shield metal arc welding (SMAW), metal inert gas (MIG) and metal active gas (MAG) welding, submerged arc welding (SAW), tungsten inert gas (TIG) welding and oxyacetylene gas welding (GW). The objectives of hardfacing are to reduce wear, build/repair metal surface, extend life time of equipment and prevent accidents[1-3].

In the present day, hardfacing is an important process for many heavy machines used in agriculture, mining, and metal industries, because of abrasive wear resistance and economic reasons. In sugarcane industry, a large number of hardfacing SMAW electrodes are used for the shredder hammers, which are made from St52-3 steel and used to crush sugarcane into small pieces. After operation for some weeks, it was observed that the surface was damaged by wear due to sand and sugar cane fiber[1, 4]. To prevent or repair damaged surface of shredder hammer, hardfacing process is applied. From economic view, the most popular hardfacing process in the sugar cane industry is the SMAW process.

The hardfacing SMAW electrode specification usually followed DIN8555: E-10-UM-65-GR standard. It contains C(6.5%), Mn(0.80%), Si(0.60%),Cr(22.70%), Nb (7.00%), and Fe (balanced)[2]. This electrode is recommended for good abrasive wear resistance of shredder hammer in sugar cane industry. However, after hardfacing the shredder hammer with this electrode, it can be used around 18 days[4]. From my point of view, none of high Cr-Nb hardfacing electrodes were developed for higher abrasive wear resistance by adding Mo. From a report of hardfacing steel[5-10], molybdenum increases the strength and surface hardness by forming carbide, increasing volume fraction of carbides, and solid solution strengthening. With higher molybdenum contents of hardfacing alloy[6-8], higher yield strength as well as surface hardness of steel can be achieved.

Molybdenum can form very fine carbide[9],  $\text{Mo}_2\text{C}$ , which is harder than Cr-rich carbide[5]. Other hardfacing reports[10-11] also found that the complex carbide formed by using

the Mo-based SMAW electrode was harder than those carbides by using the Mo-free, W-based and Cr-based electrodes. Compared molybdenum with chromium, high molybdenum alloyed steel exhibits higher abrasive resistance than high chromium alloyed steel[12]. Moreover, molybdenum increase carbide nucleation sites, which results in increasing volume fraction of carbide and higher abrasive wear resistance[13-17].

In addition, it can change morphology of carbide in microstructure[14-19]. Therefore, it is interesting to modify molybdenum composition of hardfacing high chromium-niobium SMAW electrode by addition Mo for better abrasive wear resistance. The modified compositions of coated part of SMAW electrode with molybdenum were experimented in this work.

## 1.2 Objectives

To investigate the effect of molybdenum content of hardfaced surface of St52-3 steel on wear resistance by using SMAW high chromium hardfacing electrode.

## 1.3 Conceptual Framework

1.3.1 ST52-3 steel used as based material with compositions C(0.16%), Si(0.55%), Mn(1.6%), P(0.035%), S(0.035), Fe(Balance) dimension of 25 x 76 x 6.5 mm..

1.3.2 The SMAW hardfacing electrodes with 4 different compositions as follows,

1.1.1 C(7%), Mn(0.80%), Si(0.60%), Cr(22.00%), Nb(7.00%), Fe(Balance)

1.1.2 C(6 %), Mn(0.80%), Si(0.60%), Cr(22.00%), Nb(7.00%), Mo(3%),  
Fe(balance)

1.1.3 C(5%), Mn(0.80%), Si(0.60%), Cr(22.00%), Nb(7.00%), Mo(6%),  
Fe(balance)

1.1.4 C(4%), Mn(0.80%), Si(0.60%), Cr(22.00%), Nb(7.00%), Mo(9%),  
Fe(balance)

1.3.3 Three full hardfacing layer on the surface of the St52-3 steel by using SMAW electrodes from 1.3.2 are performed. The repeated 3 samples are produced for each SMAW

electrode. SMAW was performed at DCEP voltage 20 V, current 125 A, and travelling speed 25 cm/min.

1.3.4 The chemical composition of the hardfaced surfaces of the samples by emission spectrometer.

1.3.5 The hardness of the hardfaced samples were measured 1.3.2 by using the Vickers microhardness (HV) method.

1.3.6 Volume fraction of carbides followed by ASTM E562 standard are determined[20].

1.3.7 Test wear resistance of hardfaced samples from 1.3.2 is tested according to ASTM G65 procedure D[20].

1.3.8 The microstructure of samples by optical microscope, scanning electron microscope, Energy-dispersive X-ray spectroscopy (EDX), Electron probe micro-analyzer (EPMA) and X-ray Diffraction (XRD) are investigated.

#### **1.4 Research Hypothesis**

1.4.1 Hardfaced sample gets maximum abrasive wear resistance at one value of molybdenum content.


## CHAPTER II

### LITERATURE REVIEW

#### 2.1 Molybdenum

Molybdenum is metallic element which is used as an alloying element, as a metallic coating and a based metal in a variety of market such as glass industry, high temperature furnace, tool equipment, and aerospace & defense application. The important properties of molybdenum are thermal and electrical conductivity, thermal expansion, high-temperature strength, environmental stability, hardenability, weldability, toughness and resistance to abrasive wear [22-23].

**Table 2.1** Properties of molybdenum [23-24]

Physical characteristics	
Atomic Weight	95.95 g/g atom
Density	10.22 g.cm <sup>-3</sup>
Lattice Constant	a=3.1468 Å
Crystal structure	body-centered cubic
Thermal conductivity	142 W·m <sup>-1</sup> ·K <sup>-1</sup> at 20°C
Thermal expansion	4.8 μm·m <sup>-1</sup> ·K <sup>-1</sup> at 25°C
Young's modulus	329 GPa
Shear modulus	126 GPa
Bulk modulus	230 GPa
Poisson ratio	0.31
Vickers hardness	1530 MPa (156 HV)

Molybdenum is in sub-group VI A/B of the periodic table, and in the second series of transition elements. Transition elements are those which have an incomplete inner orbit in their atomic structure.

Molybdenum improves strength of alloys by create carbide particle such as  $\text{Mo}_2\text{C}$  to resist abrasive wear [10,25]. By adding molybdenum finer microstructure, better weldability, better mechanical properties can be obtained [26].

## **2.2 Abrasive wear**

Abrasive wear occurs when one or more solid objects are loaded against particle of the object which have equal or greater hardness. It is loss of material. Tools in present day such as conveyor screws, pump impeller, shear blade, chains, mill hammers have problem with abrasive wear. Even if bulk machine is very soft, can be cause by abrasive wear. For example sugarcane, is associated with abrasive wear of shredders hammer because of small silica in sugarcane fibers [27].

The difficult of abrasive wear to be controlled is the term of “abrasive wear” cannot exactly explain the mechanism of it. Abrasive wear has 4 type.

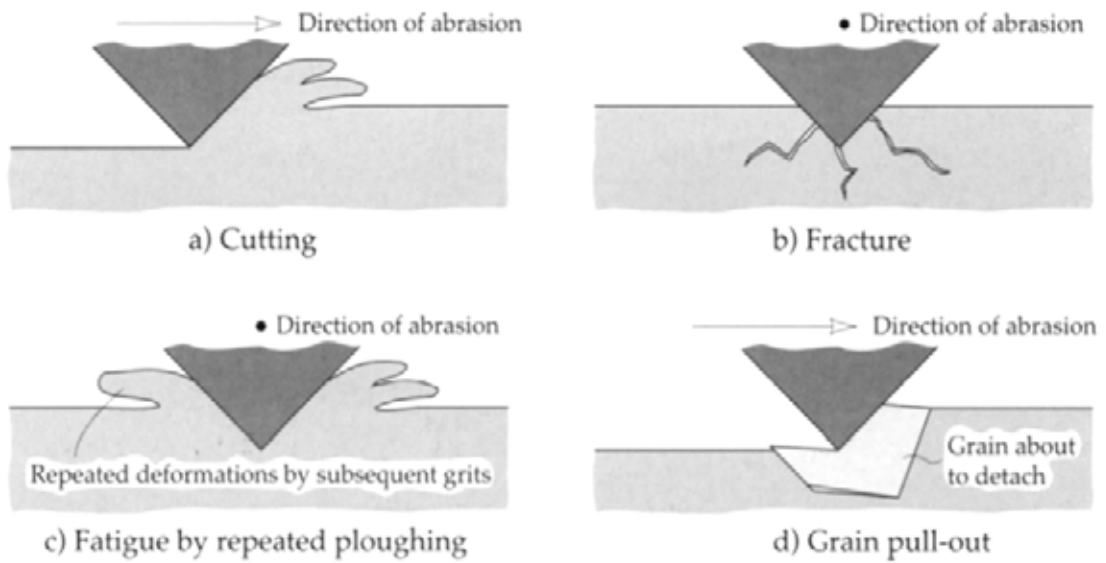


**Figure 2.1** Type of abrasive wear [27]

### 2.2.1 Cutting or Scratching

This type of abrasive wear commonly occurs by a grit or particle on surface. It is dragged along on soft metal surface under load applied usually occur when lubricant is not present. Geometry of grit affected mechanism of abrasive wear too.

### 2.2.2 Fracture

Fracture is usually generated by high load acting on brittle surface with a sharp edges grit and crack occurs.

### 2.2.3 Fatigue

Repeated strain caused by grit on surface makes metal fatigue.

### 2.2.4 Grain pull-out

Grain pull-out is commonly found on ceramics but rarely in metal. This occurs because inter-grain bonding is weak.

### 2.3 Shredder Hammer

A shredder hammer is placed at the head of a tandem, after knives and before the first hammer mill, as shown in Figure 2.2. This hammer works on cane deprived of part of its juice, and with its fibers partly disintegrated [1]. These reasons cause abrasive wear to occur on the shredder hammer. It makes the hammer mill use less power when crushing cane. The space between the anvil-bars and rotating hammer is on the order of millimeters. The shredder hammer is shown in Figure 2.3.

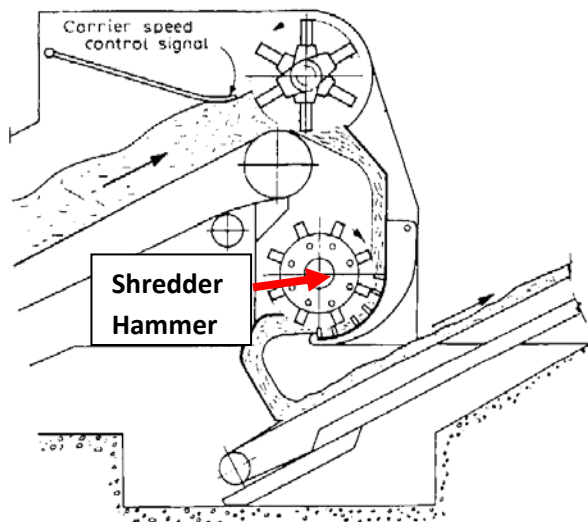


**Figure 2.2** Position of shredder hammer [1]



**Figure 2.3** Shredder hammer

From reports of sugar cane industry, the most popular welding electrode is DIN8555:E-10-UM-65-GR containing C(6.5%), Mn(0.80%), Si(0.60%),Cr(22.70%), Nb (7.00%), and Fe (balanced)[2]. This electrode can give a good preventing in abrasion, but it can be used only around 18 days in sugar cane industry[4].





**Figure 2.4** Shredder hammer after use 18 days (a) Top view (b) Side view (c) Front view

## 2.4 Shield metal arc welding

Shield metal arc welding or SMAW is one of simple, cheap, and most widely used of versatile process for fusion welding. SMAW use a covered stick electrode to weld workpieces [28]. Working process shown in Figure 2.5

SMAW is an arc welding process which melt metals is produced by heat from an electric arc that is maintained between the tip of a covered electrode and the surface of the base metal in the joint being welded.

The covered electrode consists of core wire which is drawn metal core stick or cast materials or alloys depend on standard. This core wire covers with powder materials such as fluoride, cellulose, metal alloy, and oxide. Primary function of covered electrode is a source of a stabilizers, gases to air, prevents metal and slag, insulate the hot weld metal, and consumable.

Welding arc is ignited by direct contact of electrode and work piece and short circuit occurs. This short circuit creates high density current in contact area and work piece become melt [29].

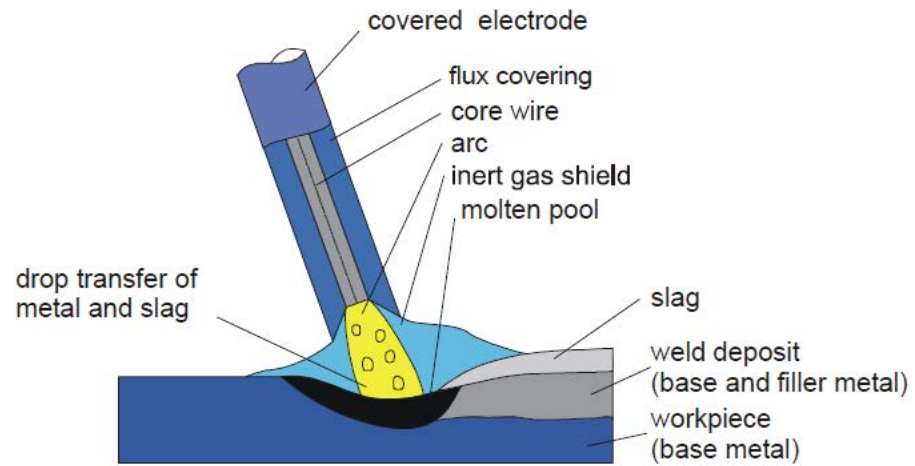


**Figure 2.5** Shield metal arc welding process[29]

The electrode and the work are part of an electric circuit illustrated in Figure 2.6. This circuit begins with the electric power source and includes the welding cables, an electrode holder, a workpiece connection, the workpiece, and an arc welding electrode.

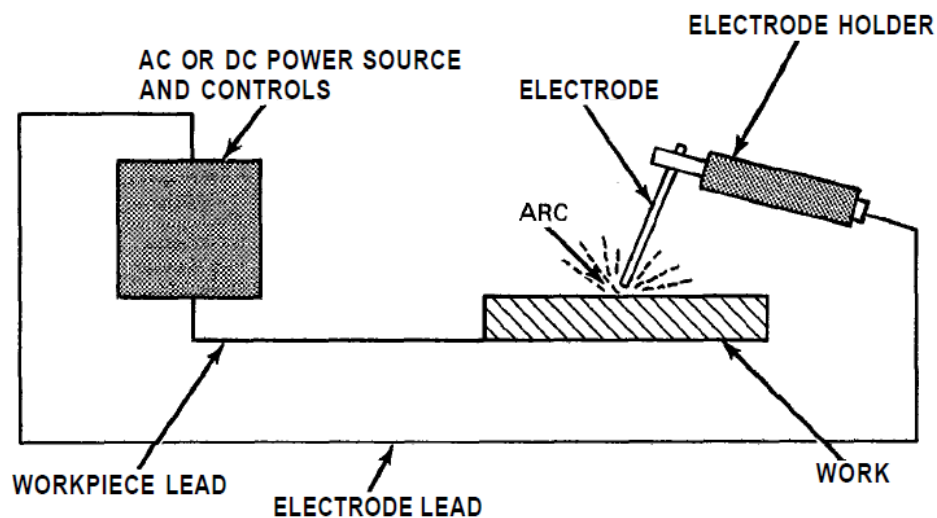


**Figure 2.6** Shield metal arc welding circuit [30]

The process requires sufficient electric current to melt both the electrode and a proper amount of base metal. It also requires an appropriate gap between the tip of the electrode and the base metal or the molten weld pool [30].

## **2.5 Hardfacing**

Nowadays, equipment is thrown away because it no longer to use which worth a lot of money. In many times the degeneration of the equipment could be stopped if use welding to repair or extend life. Hardfacing is one form of preventative maintenance welding process. The typical components that use hardfacing are buckets, crusher jaws, sugar mill roller, shredder hammer, and etc. The standard welding which can hardfacing are gas shield metal arc welding(GMAW), submerge arc welding(SAW), flux cored arc welding(FCAW), and shield metal arc welding(SMAW) [31]. The most important welding process for hardfaing is SMAW because it has widest selection alloy and wide range of materials.

Hardfacing is a technique which involves applying a layer of hard materials on surface of base metal for increasing wear and corrosion resistance of base metal. Most hardfacing materials are very hard and have a tendency to crack. Flux of hardfacing has 2 types. They are basic and rutile because these types give good toughness after welding.

### **2.5.1 Preheating**

Part of machine usually made from cast steel or alloy steel. With the high hardness of hardfacing material could make crack occurs on the part surface. Since use preheating can prevent crack on surface. Temperature of preheating depends on composition of parts or components[31]. For example Austenitic stainless steel have coefficient of expansion approximately 50% greater than cast manganese steel, distortion can be problem. Therefore, preheating should not be applied. Ferritic steels need to be preheated about 200°C or less. Martensitic steels should be preheated at 200-300 °C and slow cooling after welding [31]

### 2.5.2 Dilution

Change in chemical composition of welding filler metal by mixing with base metal during welding process called “Dilution”. Dilution can reduce lower hardness of surfacing material or absorb atom such as carbon, increased hardness and possible to have crack under weld seam.

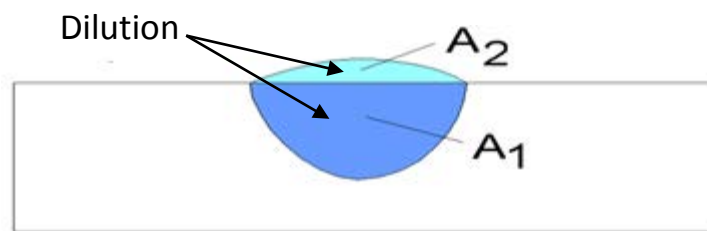


**Figure 2.7** Dilution in welding seam [29]

$$\% \text{dilution} = \left( \frac{A_1}{A_1 + A_2} \right) \times 100 \quad (2.1)$$

### 2.5.3 Relief checking

Relief checking is small cracks which formed across weld bead to break up and reduce stress. Many hardfacing materials have relief checking on cooling process. Relief checking occurs in high hardness with hardfacing alloys as a result of a large difference between the rate of expansion and contraction between it and the base material. Distortion can be controlled by relief checking. These relief checking doesn't cause detrimental to the performance of hardfacing materials. Relief checking can be minimized if high preheat temperatures are used and cooling occurs at a very slow rate[31].

## 2.6 Strengthening

### 2.6.1 Solid solution strengthening

Alloying with impurity atoms which goes into substitutional or interstitial solid solution. This is called “solid solution strengthening”. Increasing the concentration of the hard impurity results in increase in strengths. Alloys are stronger than pure metals because impurity atoms that go into solid solution ordinarily impose lattice strains on the surrounding host atoms. Lattice strain field interactions between dislocations and these impurity atoms result, and, consequently, dislocation movement is restricted [32].

### 2.6.2 Precipitation strengthening [32]

The strength and hardness of some metal alloys can be enhanced by the formation of extremely small uniformly dispersed particles of a second phase within the original phase matrix. This must be accomplished by phase transformations that are induced by heat. The process is called precipitation hardening because the small particles of the new phase are termed “precipitates”. Precipitate usually occurs in Heat-affected zone by forming  $M_xC_x$ .

**Table 2.2** Characteristics of alloy carbides usually found [33]

Type of carbide	Lattice type	Remarks
$M_3C$	Orthorhombic	This is a carbide of the cementite ( $Fe_3C$ ) type, M, maybe Fe, Mn, Cr with a little W, Mo, V.
$M_7C_3$	Hexagonal	Mostly found in Cr alloy steels. Resistant to dissolution at higher temperatures. Hard and abrasion resistant. Found as a product of tempering high-speed steels.
$M_{23}C_6$	Face-centered cubic	Present in high-Cr steels and all high-speed steels. The Cr can be replaced with Fe to yield carbides with W and Mo.
$M_6C$	Face-centered cubic	W- or Mo-rich carbide. May contain moderate amounts of Cr, V, Co. Present in all high-speed steels. Extremely abrasion

		resistant.
$M_2C$	Hexagonal	W- or Mo-rich carbide of the $W_2C$ type. Appears after temper. Can dissolve a considerable amount of Cr.
MC	Face-centered cubic	V-rich carbide. Resists dissolution. Small amount that does dissolve reprecipitates on secondary hardening.

## 2.7 Testing machine

### 2.7.1 Abrasive wear testing [21]

There are a lot of testing method to find out abrasive wear on surface such as ring on disk, pin on disk, ASTM G65. In this thesis use ATSM G65: measuring abrasion using the dry sand/rubber wheel. ASTM G65 can use sand or silica sand in testing process which is the same as sand in sugar cane. ASTM G65 test results are reported as volume loss. Abrasive wear occurs between the sample and a wheel. The sample is loaded against the wheel with specified force. Testing machine is shown in Figure 2.7

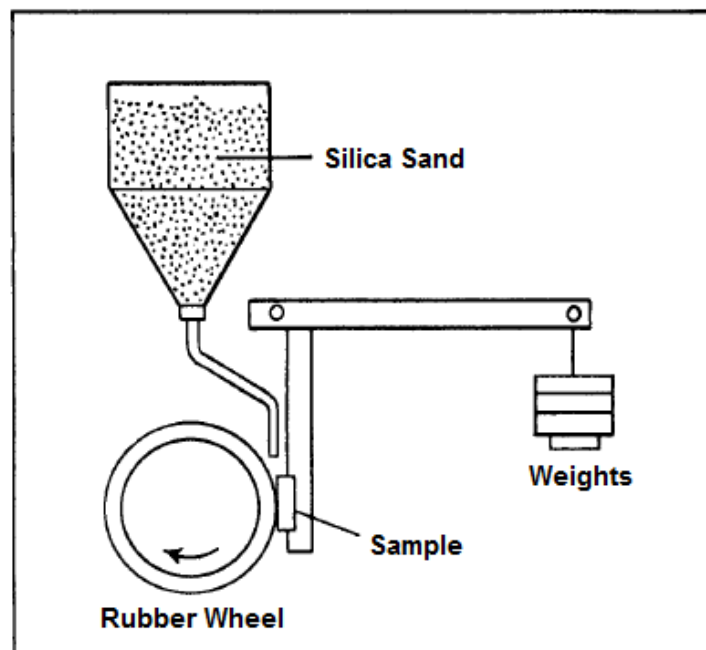


Figure 2.8 ASTM G65 testing machine[21]

The volume loss can define by equation

$$\text{Volume loss (mm}^3\text{)} = \left( \frac{\text{mass loss (g)}}{\text{density of specimen (}\frac{\text{g}}{\text{cm}^3}\text{)}} \right) \times 1000 \quad (2.2)$$

Abrasive wear resistance defined by

$$\text{Abrasive wear resistance (}\frac{\text{mm}^3}{\text{m}}\text{)}^{-1} = \left( \frac{\text{volume loss (mm}^3\text{)}}{\text{sliding distance (m)}} \right)^{-1} \quad (2.3)$$

### 2.7.2 Microstructure analysis

To investigate particles of carbide on the hardfacing surface, we can use optical microscope. Since most of carbide have particle size about 200  $\mu\text{m}$ . [5, 34], range of optical microscope is enough to observe carbide. Optical microscope use reflex technique to observe microstructure of material as shown in Figure 2.8

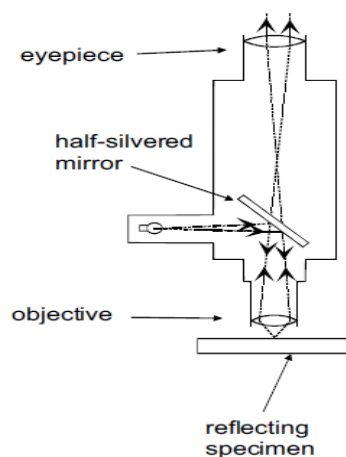


**Figure 2.9** Optical microscope [35]

## **2.8 Relevant research**

In 2005, M.F. Buchely and group [11] studied effect of microstructure on abrasive wear of hardfacing alloys. The samples are Cr-rich, W-rich, and complex carbides hardfacing alloys. Those are 3-layer welded on ASTM A36 steel plates. There are 3 experimental. The first experiment is hardness measurements by using load 0.3 kgf. Hardness results showed complex carbide harder than W-rich and W-rich harder and Cr-rich respectively as shown in Table 2.3. The second experiment is microstructure analysis which used optical and scanning electron microscopes. The result shown in Figure 2.9



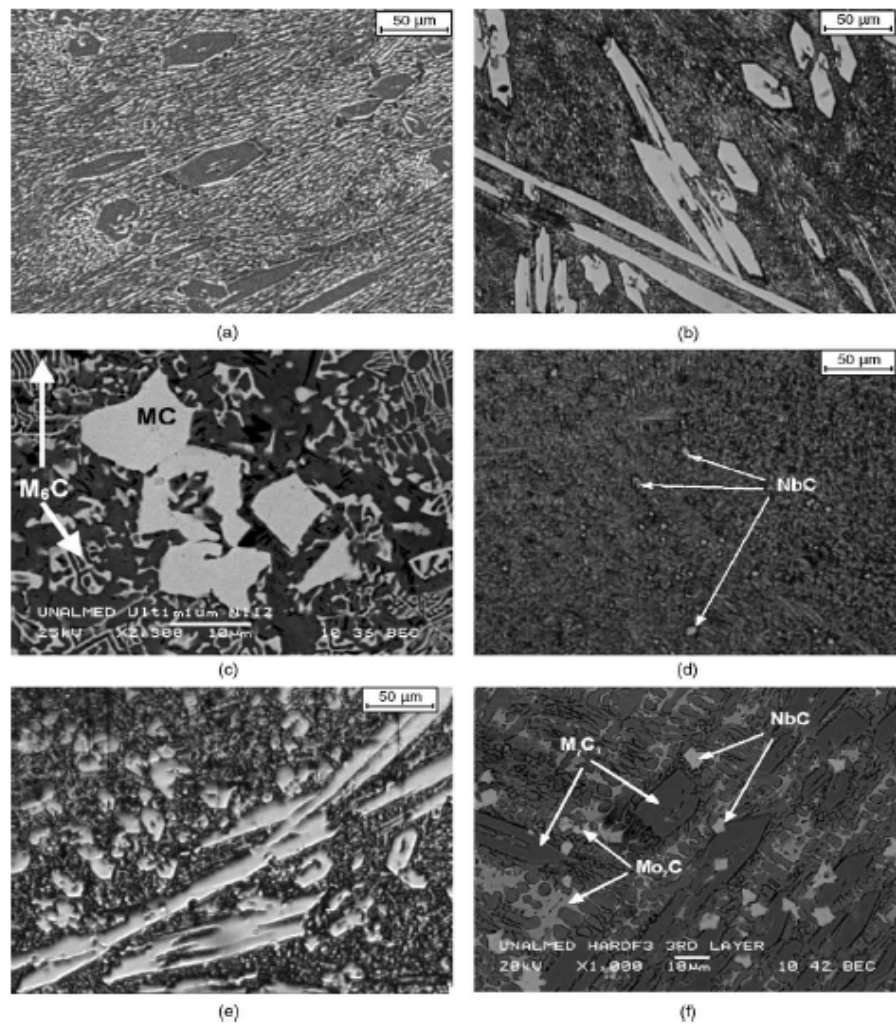


**Figure 2.10** Hardfacing microstructure: (a) Cr-rich, first layer (b) Cr-rich, second layer (c) W-rich layer (d) complex carbides, first layer (e) complex carbides, second layer (f) complex carbides, third layer. Images (a), (b), (d) and (e) were using optical microscope and image (c) and (f) were using SEM

**Table 2.3** Hardness of deposit materials

	Hardfacing 1 (Cr-rich)		Hardfacing 2 (W-rich)	Hardfacing 3 (complex carbides)		
	1st layer	2nd layer	1st layer	1st layer	2nd layer	3rd layer
Hardness (HRC)						
Sample 1	55.7	57.0	58.6	51.8	56.8	60.5
Sample 2	55.4	58.0	58.0	55.0	60.1	59.5
Sample 3	-	-	58.3	56.9	59.9	60.5
Average	55.6	57.5	58.3	54.6	58.9	60.2

From Figure 2.9, Cr-rich deposits have  $M_7C_3$ -type chromium carbides. W-rich deposit is composed by MC-type carbides surrounded by  $M_6C$ -type carbide. Lately, complex carbides deposit with  $M_7C_3$ , Nb-rich MC, Mo-rich  $M_2C$ , and W-rich WC carbides. The third experiment is abrasive wear test. Abrasive wear was test by quartz particle mean diameter between 212 and 300  $\mu\text{m}$  on ASTM G65 standard. Conditions of ASTM G65 are load 130 N, velocity 200 rpm, and wear distance 4309 m. The results shown in Table 2.4

**Table 2.4** General results from dry wheel ASTM G65

Hardfacing	Cr-rich, 1st layer	Cr-rich, 2nd layer	W-rich, 1st layer	Complex carbides, 1st layer	Complex carbides, 2nd layer	Complex carbides, 3rd layer
Mass loss (mg)	292.38	151.9	177.9	385.4	278.5	147.1
Volume loss <sup>a</sup> ( $\text{mm}^3$ )	37.5	19.5	22.8	49.4	35.7	18.8
Abrasive wear resistance <sup>b</sup> ( $\text{mg m}^{-1}$ ) <sup>-1</sup>	14.7	28.4	24.2	11.2	15.5	32.3
Abrasive wear resistance <sup>b</sup> ( $\text{mm}^3 \text{m}^{-1}$ ) <sup>-1</sup>	114.9	221.3	188.9	87.2	120.7	228.5

<sup>a</sup> Average density estimated:  $7.8 \text{ g cm}^{-3}$ .

<sup>b</sup> Defined as volume loss/sliding distance.

From Table 2.4 and Figure 2.9 found that the best abrasive wear resistance can receive from complex carbide because this complex carbide has coarse  $M_7C_3$ -type carbide and reinforced by NbC carbides particles. According to Table 2.3 and 2.4, relation between hardness and abrasion resistance can be shown in Figure 2.10. These relations showed that abrasion resistance depends on hardness.

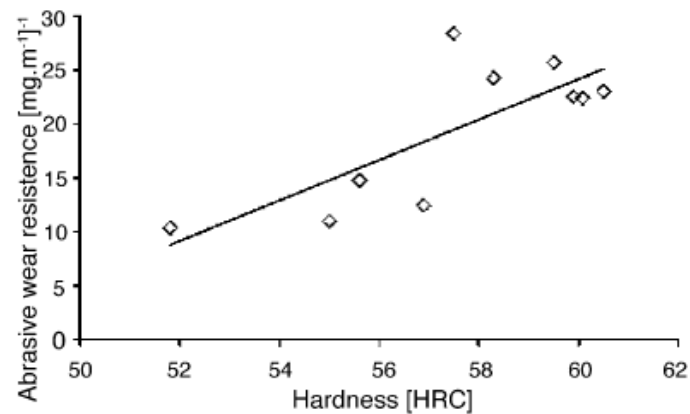


**Figure 2.11** Relation between hardness and abrasion resistance

In conclusion, the complex carbide deposits give the best abrasive wear resistance of all hardfacing alloy.

In 2008, X.H. Wang and group [10] studied effect of molybdenum on the microstructure and wear resistance of Fe-based hardfacing coating. The hardfacing samples are different by varied Fe-Mo powder in composition as shown in Table 2.5

**Table 2.5** Composition (wt-%) of hardfacing electrode

Samples	Fe-Ti	Fe-V	Fe-Mo	Graphite	CaCO <sub>3</sub>	TiO <sub>2</sub>	CaF <sub>2</sub>
S1	15	12	0	10	10	30	12
S2	15	12	2	10	10	30	12
S3	15	12	3	10	10	30	12
S4	15	12	4	10	10	30	12
S5	15	12	5	10	10	30	12

The hardfacing was deposited on AISI1020 by using four layer, current 170A, arc voltage 20-25V, and travel speed 25-28 cm/min. Experiment divided to 3 parts. First experiment is investigating on microstructure. All sample were etched with 3% nital after that the microstructure were observed by SEM and TEM with EDS. The SEM morphology of all samples is shown in Figure 2.11. In Figure 2.11 shows effect of amount of Fe-Mo on microstructure. Figure 2.11(b-e) the carbide exist and size of it depends on amount of Fe-Mo. In Figure 2.11(e) Fe-Mo is more than 6wt-%, network of carbide occurred on grain boundary. In Figure 2.12 shows the X-ray diffraction spectrum of sample S4 and S1. In the S4 hardfacing layer contains TiC, VC, Fe<sub>3</sub>C,  $\alpha$  - Fe and Mo<sub>2</sub>C.

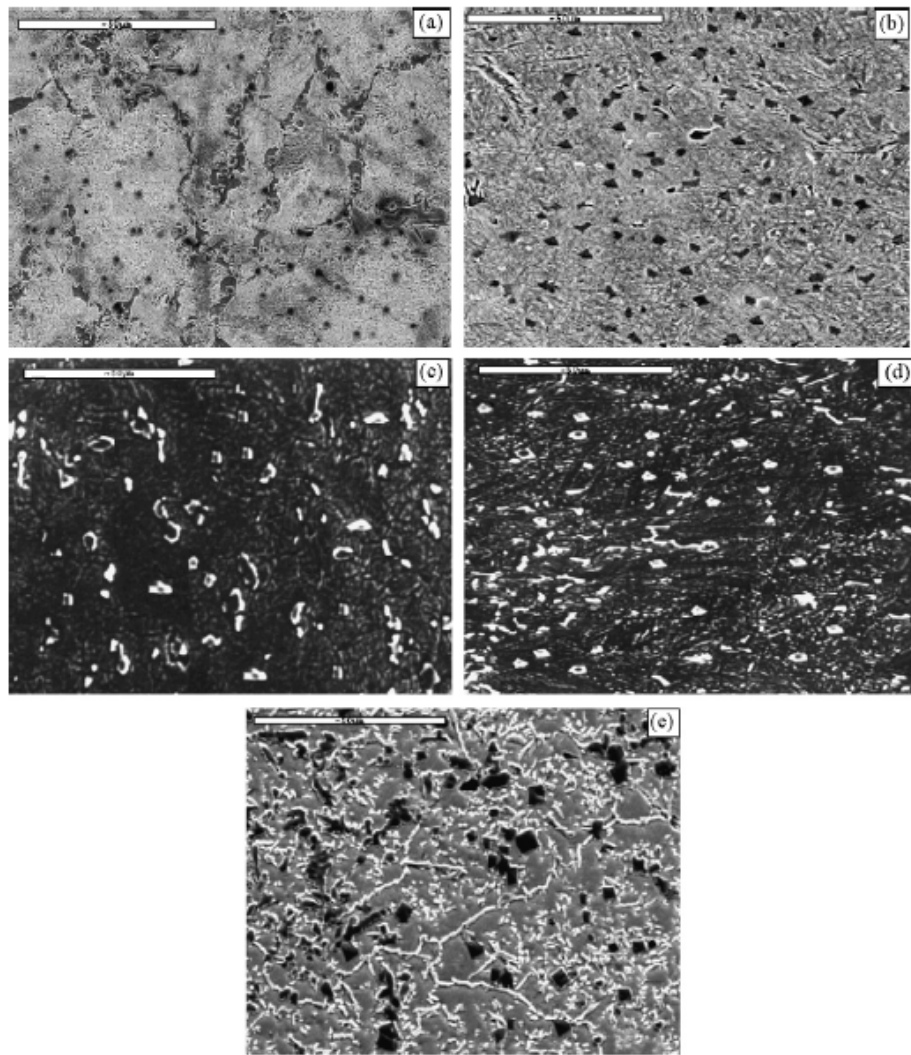


**Figure 2.12** SEM morphology of the S4 hardfacing layer

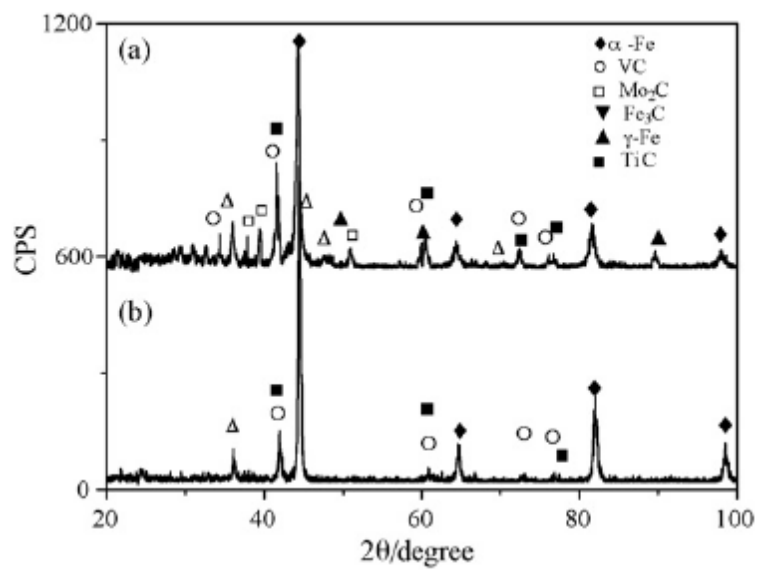


**Figure 2.13** X-ray diffraction spectrum of hardfacing layer (a) S4-specimen and (b) S1-specimen

The carbide and precipitated in matrix is investigated by TEM as shown in Figure 2.13

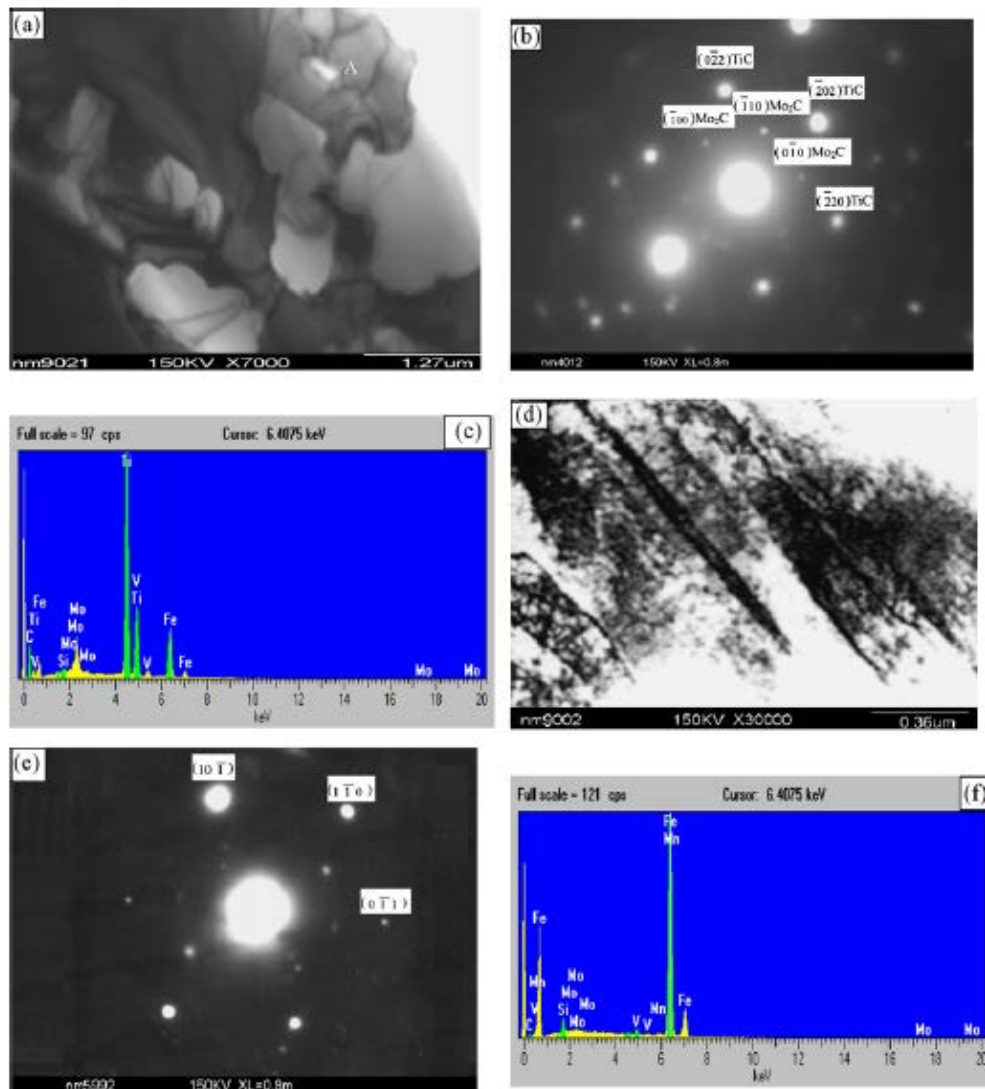


**Figure 2.14** TEM image of the hardfacing layer (a) image of carbide, (b) electron diffraction pattern of TiC-Mo<sub>2</sub>C, (c) EDS for carbide, (d) image of lath martensite matrix, (e) electron pattern of matrix, and (f) EDS for matrix

The TEM results show that carbide contains mainly C, Ti, V, and Mo in Figure 2.13(c). On the other hand, in Figure 2.13(f) Mo is not combined with C but dissolved in the matrix. Because of that matrix is strengthened by solid-solution strengthening.

The second experiment is wear resistance test by using block-on-ring method the results shown in Figure 2.14. It shows that the volume loss decrease when amount Fe-Mo increase because carbide in hardfacing layer increase.

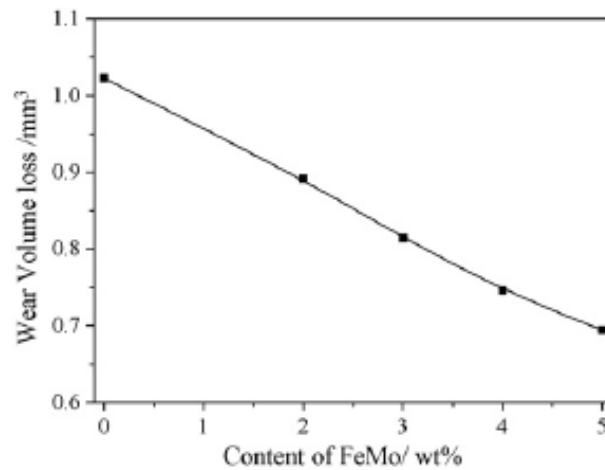


**Figure 2.15** Effect of the amount of Fe-Mo on wear volume loss

Third experiment is measuring the macrohardness by using Rockwell scale C method. Macrohardness of each samples are shown in Figure 2.16. It shows that more amount of Fe-Mo in wt-% more hardness gain because more carbides are formed.

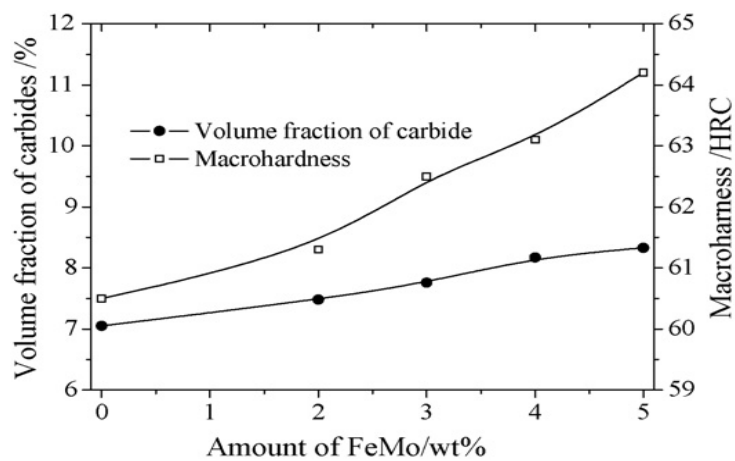


**Figure 2.16** Effect of the amount of Fe-Mo on macrohardness and volume fraction of carbides



In conclusion complex carbide of TiC-VC-Mo<sub>2</sub>C reinforced Fe-Based hardfacing layers by forming carbide and higher Mo content more wear resistance gain.

In 2008 , X. Zhang and group [26] studied effect of molybdenum on microstructure and mechanical properties of ultrafine Ti(C,N) based cermets. Samples were prepared by using WC, Mo, Co, C, ultra-fine Ti(C,N) mixed powder and latex binder. Green compact were made by uniaxial pressing. After that sintering under vacuum at 1430°C for 1 hour. The chemical composition of design experiment materials are shown in table 2.6

**Table 2.6** Chemical composition design of experimental materials.

Specimen	Mo	Ti(C,N)	WC	Co	C
A	0	62.5	20	15	2.5
B	5	57.5	20	15	2.5
C	10	52.5	20	15	2.5
D	15	47.5	20	15	2.5
E	20	42.5	20	15	2.5

Figure 2.17 shows microstructures of all specimen. From figure 2.17, it can be seen that bright core amount increase with molybdenum content. In addition, grain refining effect shows on this figure. Molybdenum increase wettability between ceramic and metallic phase. Dissolution of Ti(C,N) grains can be decrease by increasing molybdenum content and make grain stop growth. This may probably occurred because molybdenum created shell. Average grain size is shown in table 2.7.

**Table 2.7** Average gain size of experimental cermets.

Specimen	A	B	C	D	E
Grain size(μm)	1.23	1.17	1.15	0.79	0.88

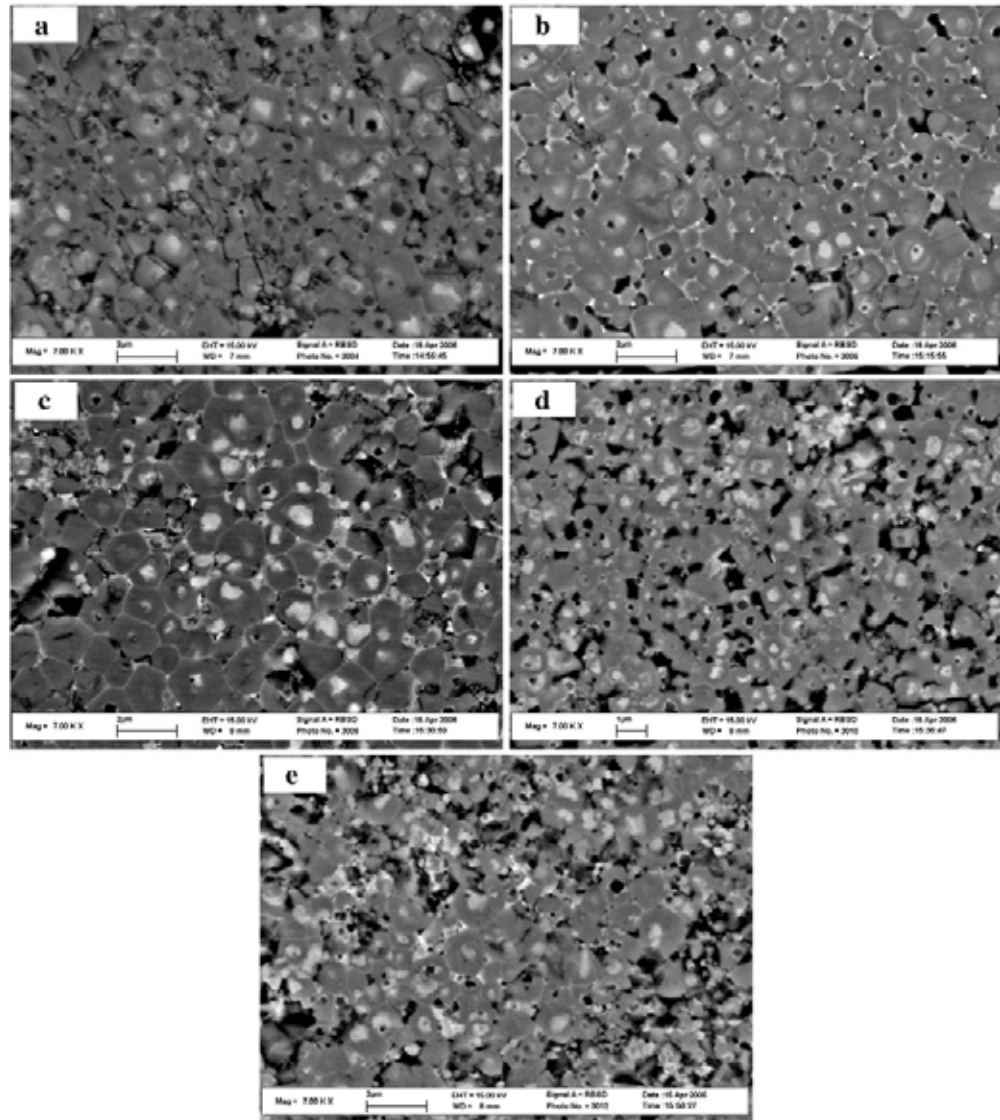


**Figure 2.17** SEM-BSE micrographs of microstructure with different molybdenum content(wt-%).

(a) 0%Mo, (b) 5%Mo, (c) 10%Mo,(d) 15%Mo, (e) 20%Mo.

Transverse rupture strength, hardness and fracture toughness of specimen were tested in experiment. Figure 2.18 shows effects of molybdenum content on transverse rupture strength. Trend of rupture strength are increased with molybdenum increase and a peak value is at 15 wt-% of molybdenum. Molybdenum increase rupture strength because it improve wettability, decrease grain size of cermets, and provide solid solution strengthening effect.

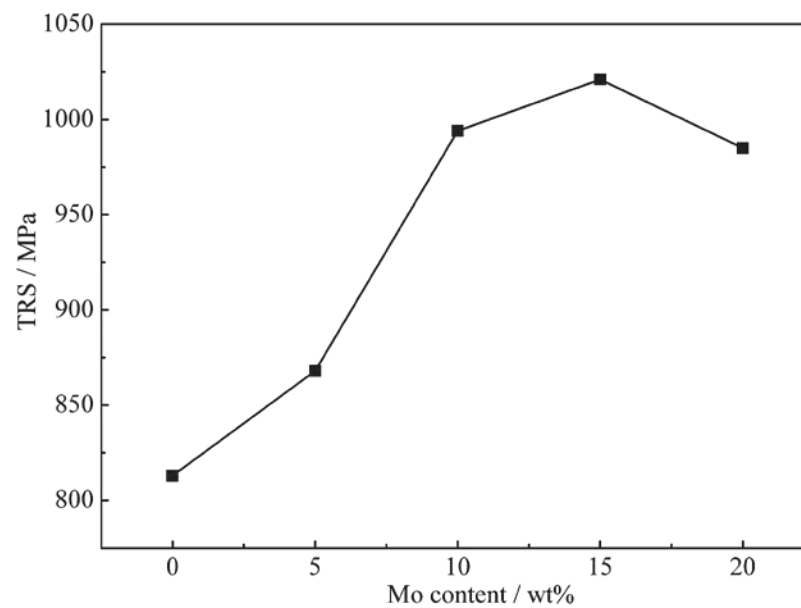


**Figure 2.18** The effect of Mo content on rupture strength

Hardness of cermets were tested by Rockwell hardness scale A method (HRA) shows in figure 2.19. Hardness increase with molybdenum content. This is because molybdenum provide grain refining effect.

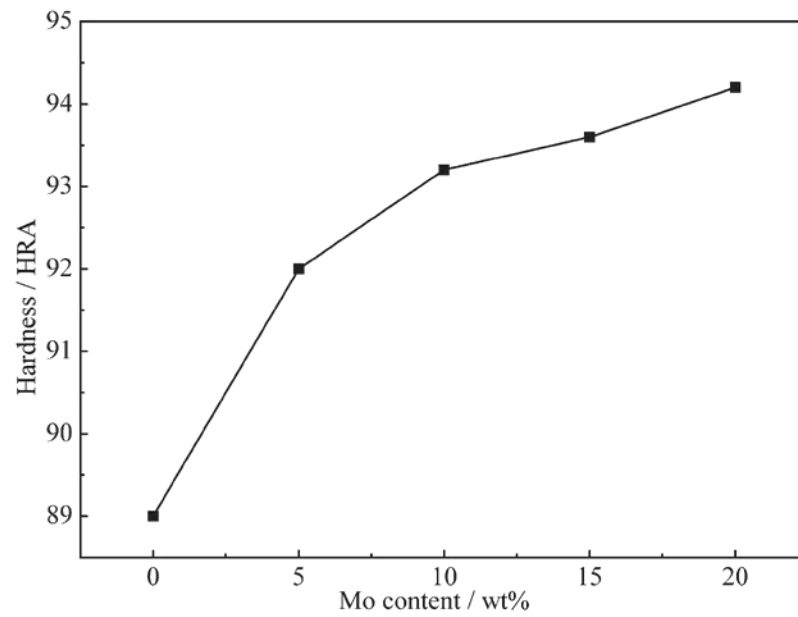


**Figure 2.19** The effect on Mo content on hardness.

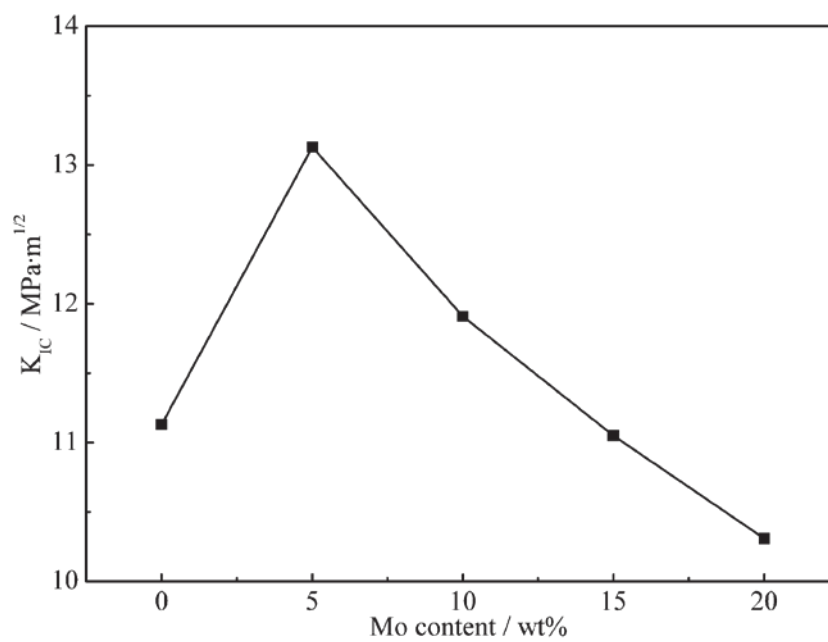


**Figure 2.20** The effect on Mo content on fracture toughness.

The fracture toughness has peak at molybdenum equal 5 wt-%. At low content of molybdenum, it provide solid solution strengthening effect after that increasing molybdenum content causes too much hardening.

In conclusion, molybdenum improve wettability between ceramic and metallic phase and decrease solubility of Ti(C,N) in the binder stop grain growth. It can also increase rupture strength and hardness as well as toughness. For toughness it can be only increase when molybdenum content is low.

In 2005, M.X. Yao and group [17] studied Wear, corrosion and cracking resistance of some W- or Mo-containing Stellite hardfacing alloys. Low and high stress abrasive wear test was carried out by ASTM G65 under procedure B and use soft-steel wheel in high stress test instead of rubber wheel. Abrasive particle is AFS 50/70 Ottawa sand. The samples were coated by plasma transferred arc-welding method with different powder. The chemical compositions of powder are shown in table 2.8

**Table 2.8** Nominal compositions of Co–Cr–W–C and Co–Cr–Mo–C Stellite alloys

Alloy	Type	Cr	W	Mo	C
Stellite 6	Co–Cr–W–C	29	4.5	-	1.2
Stellite 706	Co–Cr–Mo–C	29	-	4.5	1.2
Stellite 12	Co–Cr–W–C	29	8	-	1.8
Stellite 712	Co–Cr–Mo–C	29	-	8	1.8
Stellite 1	Co–Cr–W–C	30	12	-	2.5
Stellite 701	Co–Cr–Mo–C	30	-	12	2.5
Stellite 190	Co–Cr–W–C	26	14	-	3.2
Stellite 790	Co–Cr–Mo–C	26	-	14	3.2

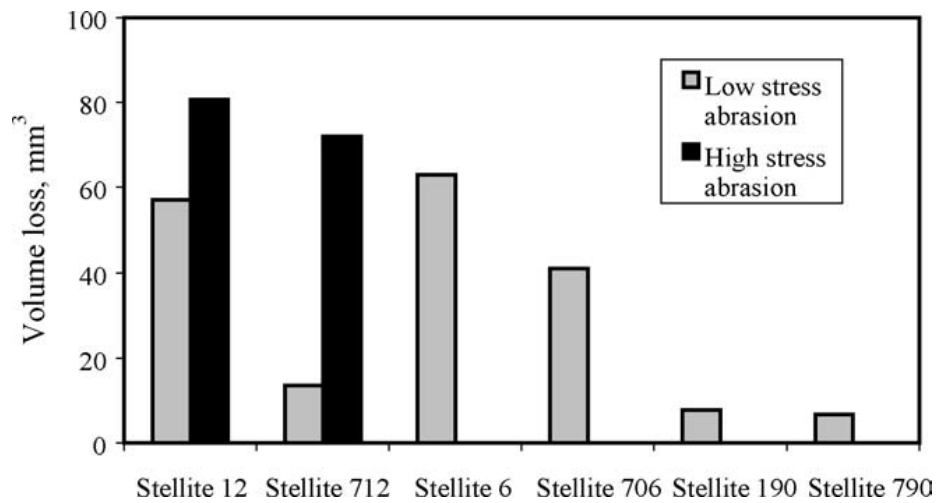


**Figure 2.21** Low-stress abrasive and high-stress abrasive-wear resistance.

From figure 2.21, it can be seen that volume loss decrease with molybdenum content increase. Scratch test was used to find cracking resistance. The testing was run on an automatic scratch tester with a diamond Rockwell C indenter. After applied force 20 N. to critical load the cracks were appeared and SEM of samples are shown in figure 2.22. The calculated critical plastic strain for each test is shown in figure 2.23.

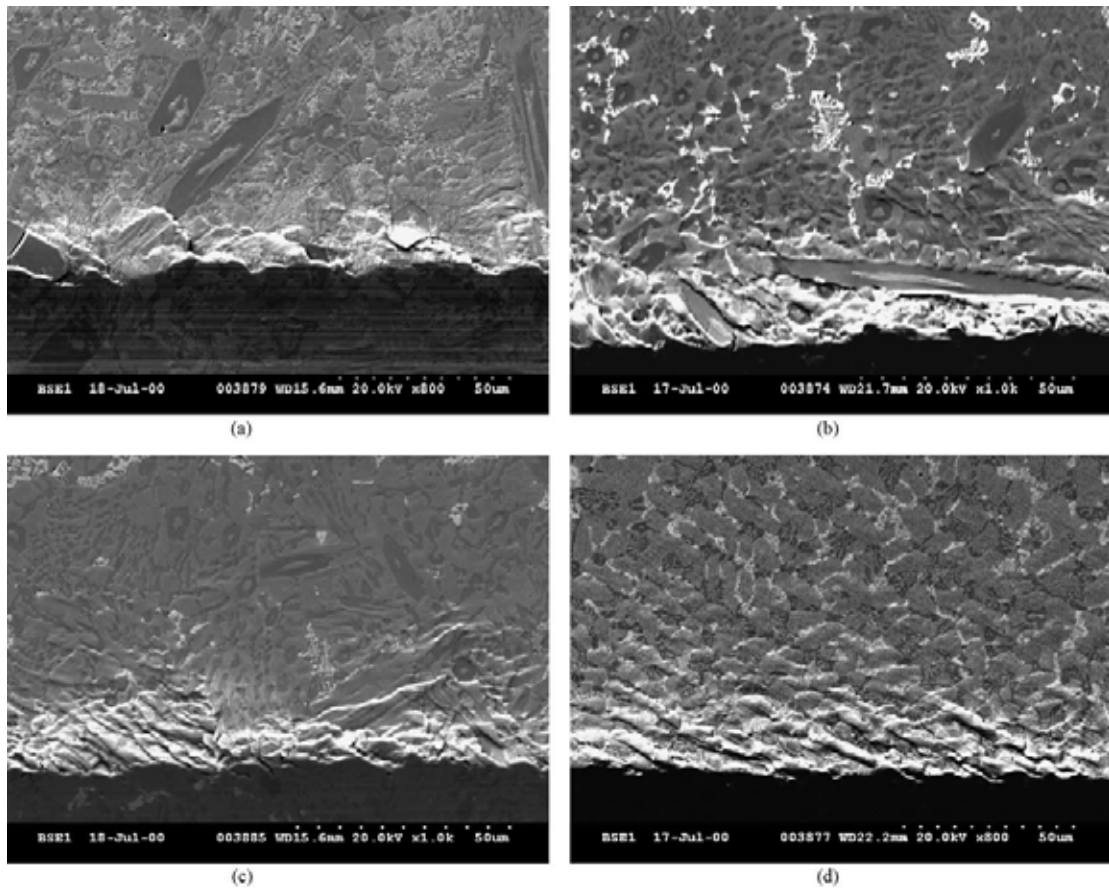


**Figure 2.22** SEM images of the scratches made above the critical load. Scratch direction was from left to right. (a) Stellite 790 at normal load of 95N with plastic strain of 0.32; (b) Stellite 190 at normal load of 110N with plastic strain of 0.40; (c) Stellite 1 at normal load of 88N with plastic strain of 0.34, and (d) Stellite 701 at normal load of 62N with plastic strain of 0.31.

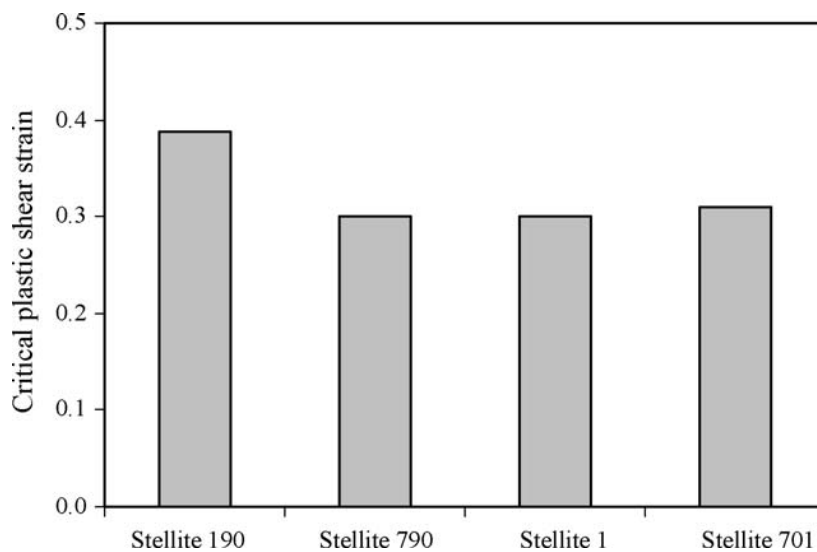


**Figure 2.23** Cracking resistance in terms of critical plastic shear strain.

From figure 2.22 and figure 2.23, it shows that the sample with 14 wt-% Mo have slightly higher crack resistance 12wt-% Mo sample. Molybdenum alloying effect in Stellite alloy by change carbide morphology and increase volume fraction of carbides in microstructure more than tungsten because molybdenum atoms are lighter than tungsten atom.



## CHAPTER III

### METHODOLOGY

#### 3.1 Materials

##### 3.1.1 St52-3 steel

The base material used was St52-3 steel. Its composition is shown in Table 3.1.

**Table 3.1** Chemical composition of St52-3 DIN17100 steel by emission spectrometer

Chemical Elements	C	Si	Mn	P	S	Fe
(wt-%)	0.137	0.310	1.352	0.024	0.015	Balance

##### 3.1.2 SMAW hardfacing electrode

The designed SMAW hardfacing electrodes were prepared by the Zika Industries Company Limited, Israel. The electrode flux was modified from the old version by adding different Mo contents but still keeping the same Cr and Nb compositions. After hardfacing, the designed compositions of hardfaced surface of St52-3 steel should consist of different Mo contents but constant Cr and Nb contents as shown in Table 3.2.

**Table 3.2** The designed chemical composition of hardfacing surface of St52-3 steel by SMAW

Sample	Chemical Elements (%wt.)						
	C	Si	Mn	Cr	Mo	Nb	Fe
Hardfacing electrode 1 (S1)	7	0.80	0.80	22	-	7	Balance
Hardfacing electrode 2 (S2)	6	0.80	0.80	22	3	7	Balance
Hardfacing electrode 3 (S3)	5	0.80	0.80	22	6	7	Balance
Hardfacing electrode 4 (S4)	4	0.80	0.80	22	9	7	Balance

#### 3.2 Equipment

3.2.1 Shield metal arc welding source (SMAW source)

3.2.2 Weighing scale four decimal points

3.2.3 Wire cutting machine

3.2.4 Grinding machine

3.2.5 ASTM G65 standard dry sand-rubber wheel testing machine

3.2.6 Vickers microhardness tester

3.2.7 X-ray diffractometer (XRD)

3.2.8 Optical microscope (OM)

3.2.9 Scanning electron microscope (SEM)

3.2.10 Electron probe micro-analyzer (EPMA)

3.2.11 Energy-dispersive X-ray spectrometer (EDX)

3.2.12 Emission spectrometer

### 3.3 Experimental Procedure

3.3.1 Prepare St52-3 base materials with dimension of 25 x 76 x 6.5 mm. for 16 pieces.

3.3.2 Divide samples from 3.3.1 into 4 groups. Each group contains 4 samples.

3.3.3 Full hardfacing on the surface of base metal from 3.3.2 by using the hardfacing electrode 1 as in 3.1.1.2 under condition DCEP voltage 20 V, current 120 A, and travelling speed 25 cm/min. Three hardfacing layers were prepared on the St52-3 steel as shown in Figure 3.1 for decreasing the dilution of hardfacing layer by base material. Figure 3.2 shows the base material after full hardfacing on the surface.

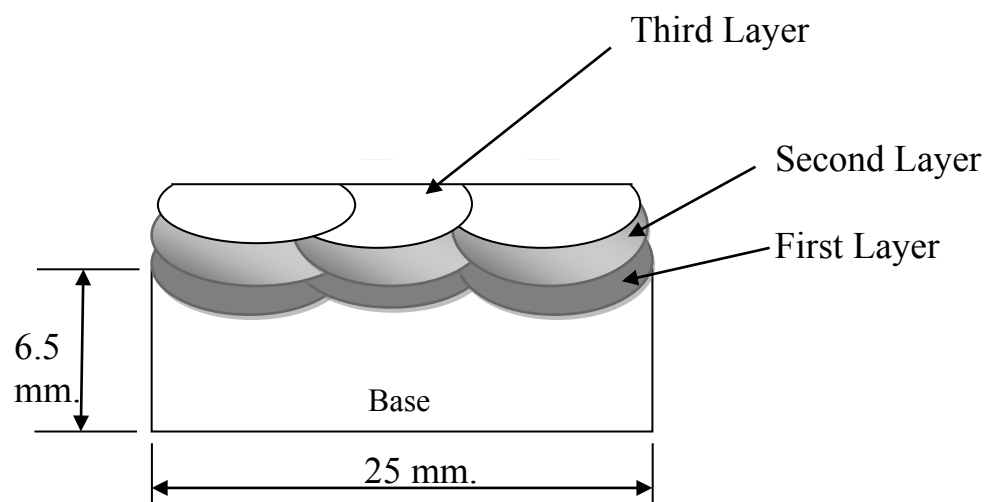


**Figure 3.1** A schematic diagram of the three hardfaced layers on St52-3 steel.



**Figure 3.2** Base material after full hardfacing on the surface.

3.3.4 Repeat 3.3.3 to the other St52-3 steel groups by using hardfacing electrodes 2, 3 and 4.

3.3.5 Check the element composition of the hardfacing surface by Emission Spectrometer

3.3.6 Grind the hardfaced surface of samples to become flat as shown in Figure 3.3.



**Figure 3.3** Flat surface of hardfaced samples after grinding.

3.3.7 Select 3 samples from each group after hardfacing and weigh by a weighing scale with four decimal points before abrasive wear test as shown in Figure 3.4.



**Figure 3.4** Weighing scale four decimal points (Mettler Toledo AB304-S)

3.3.8 Test the samples in 3.3.7 and St52-3 steel for abrasive wear resistance by ASTM G65 testing machine using dry sand-rubber wheel. The test conditions are shown in Table 3.3. Figure 3.5 shows the abrasive wear testing machine.

**Table 3.3** The abrasive wear test conditions after ASTM G65 [21].

Procedure	Load (N)	Velocity (rpm)	Wear distance (m)
D	45	200	4309

3.3.9 Weigh mass of all samples after abrasive wear test.

3.3.10 Calculate the abrasive wear resistance by using equation 3.1

$$\text{Abrasive wear resistance} = \left( \frac{\text{volume loss}}{\text{sliding distance}} \right)^{-1} \quad (3.1)$$

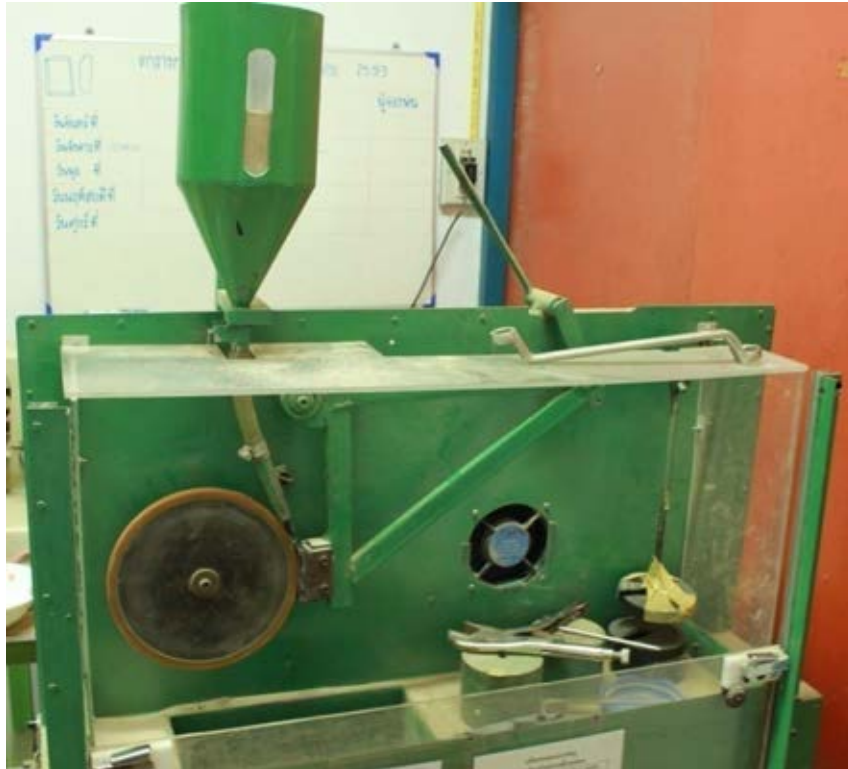


**Figure 3.5** Abrasive wear testing machine after ASTM G65 using dry sand-rubber wheel.

3.3.11 Observe the surface after wear test by SEM.

3.3.12 Cut the last sample from each group to 25 x 10 mm, with 12.5-mm thickness by wire cutting machine as shown in Figure 3.6 with cutting speed at 0.5 mm./min. under cooling condition.

3.3.13 Grind all samples in 3.3.12 with abrasive paper down to No. 2,000. Then polish with alumina powder on cross-section.

3.3.14 Etch one piece from each group samples in 3.3.13 with waterless Kalling's etching. (100 mL ethanol, 5 mL HCL, 5 g  $\text{CuCl}_2$ ) Figure 3.7 shows the example of the cross-section surface of sample for microstructure observation.

3.3.15 Observe the microstructure of all layers of samples in 3.3.14 by OM and SEM.

3.3.16 Determine the volume fraction of total carbides from OM picture by the systematic manual point counting method following ASTM E562 standard using 100 points and 30 frames for each sample.



**Figure 3.6** Wire cutting machine (Troop TP-25)

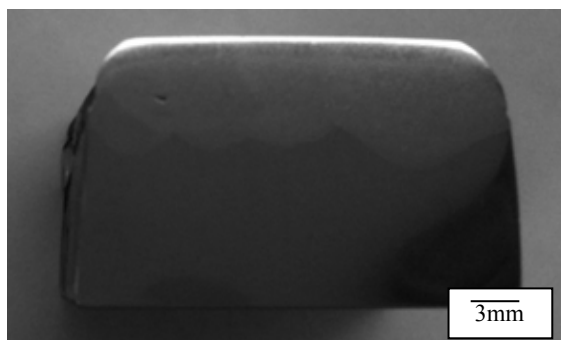


**Figure 3.7** Cross-section of hardfaced sample



**Figure 3.8** Scanning electron microscope with EDX (Jeol-5800LV)

3.3.17 Analyze the composition of microstructure by EDX spectrometer.

3.3.18 Analyze the element composition on each layer of sample S3 by EPMA as shown in Figure 3.9.

3.3.19 Measure the hardness of samples in 3.3.14 by Vickers microhardness tester as shown in figure 3.8 using 0.3 kgf for 15 second.



**Figure 3.9** Electron probe micro analyzer (Jeol JXA-8100)



**Figure 3.9** Vickers microhardness measurement machine

3.3.20 Investigate phases in the hardfaced samples in 3.3.15 by XRD using  $\text{Cu-K}\alpha$  radiation. The samples were scanned from  $5^\circ$  to  $90^\circ$  of  $2\theta$  with step of  $0.02^\circ$ .





**Figure 3.10** X-ray diffractometer (XRD) (Bruker D8 advance)

### **3.4 Analysis experiment result**

#### 3.4.1 Abrasive wear resistance

3.4.1.1 Calculate weight loss from the weight before and after wear test.

3.4.1.2 From weight in 3.4.1.1 and equation 2.1, calculate volume loss as well as abrasive wear resistance.

3.4.1.3 Analyze data from 3.4.1.2.

3.4.1.4 Compare results from 3.4.1.3 with the result of St52-3 Steel.

3.4.1.5 Take photos of abrasive wear scar on the surfaces after the test.

#### 3.4.2 Hardness measurement

3.4.2.1 Measure hardness of the hardfaced surface. Figure 3.11 shows how to measure the length of diamond pyramid cavity on microstructure.



**Figure 3.11** Measuring length of diamond pyramid cavity on microstructure

3.4.2.2 Try to correlate between hardness and abrasive wear resistance data.

### 3.4.3 Microstructure observation

3.4.3.1 Take photos of microstructure of hardfacing layer by OM, SEM and analyze element composition on the surface by EDX and EPMA.

3.4.3.2 Determine the volume fraction of carbides following ASTM E562 standard test method [20] by systematic manual point count using 100 points and 30 frames with 95% confident interval for each sample. Example of point counting grid is showed in Figure 3.12.

3.4.3.3 From XRD results, identify the carbides.

3.4.3.4 Investigate the relation between the observed carbides and the other test results.

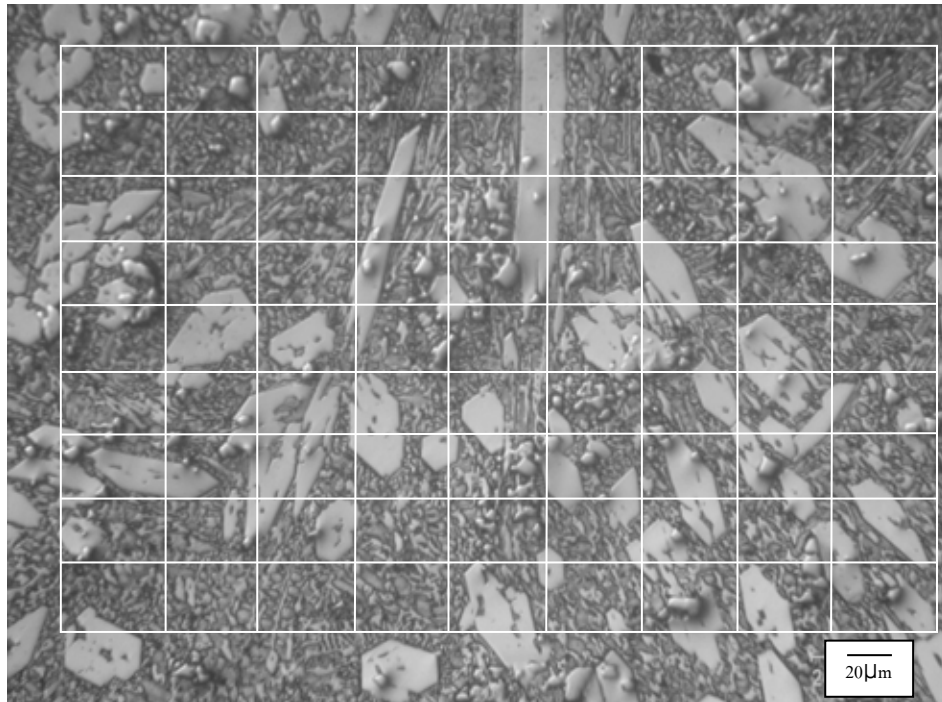


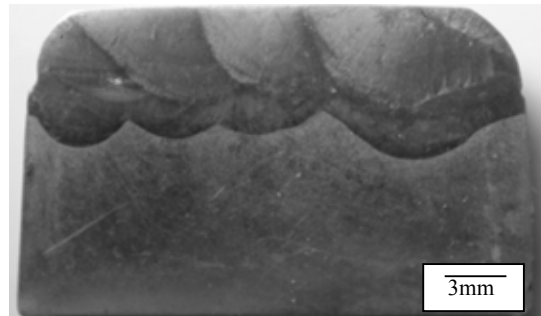
**Figure 3.12** ASTM E562 standard test method for determining volume fraction by systematic manual point count using 100 points

## CHAPTER IV

### RESULT AND DISCUSSION

#### 4.1 Microstructure analysis

In Fig. 4.1 shows the cross-section of sample after hardfacing process. It can be seen that the third layers have very large area on the surface. This means the hardfacing samples can resist the abrasive with pure chemical composition of hardfacing electrode. Typically dilution on first layer is about 50%, second layer is about 25%, and third layer gives less dilution can be less than 12.5%



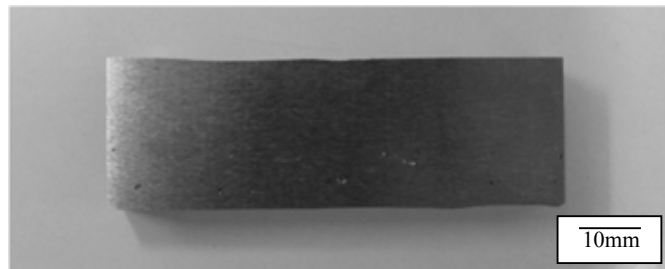
**Figure 4.1** Cross-section of sample after hardfacing.

Table 4.1 shows the chemical composition on hardfacing surface by emission spectrometer. It shows that the composition on the surfaces have big different in carbon and molybdenum contents. This could make the hardfacing surface have different phase and carbides.

**Table 4.1** Chemical composition of hardfaced surface by emission spectrometer

Top hardfaced surfaces	Chemical Elements / wt-%						
	C	Si	Mn	Cr	Mo	Nb	Fe
S1	6.99	0.80	0.84	22.80	-	7.89	Balance
S2	6.23	0.85	0.83	22.48	2.98	7.79	Balance
S3	5.23	0.92	0.83	20.40	6.43	7.19	Balance
S4	4.26	0.84	0.66	19.51	10.19	7.00	Balance

After applied the hardfacing layer, porosity appeared on surface of sample with molybdenum 10.14 wt-% as shown in Fig. 4.2. This could give poor abrasive wear resistance due to sand rapidly scratch on the edge of porosity.

**Figure 4.2** Porosity on hardfacing surface of sample S4

Microstructures of the top surface of samples S1-S4 were obtained by OM and SEM as shown in Fig. 4.3(a-d) and 4.4(a-d), respectively.

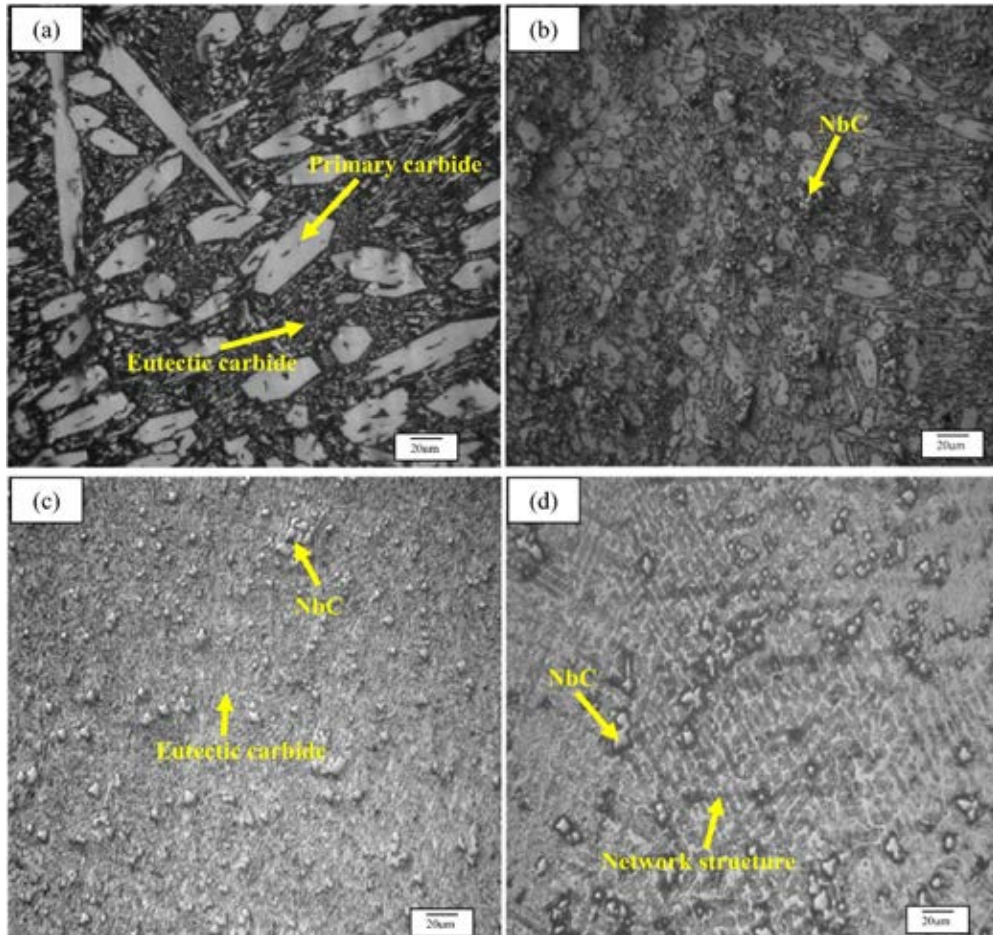


**Figure 4.3** Microstructure of the top layer of samples observed by OM (a) sample S1 (b) sample S2 (c) sample S3 (d) sample S4

All microstructures mostly consist of coarse and fine carbides, which could be  $\text{Cr}_7\text{C}_3$ , NbC,  $\text{Mo}_2\text{C}$  or mixed metal carbides [22]. The coarse carbides shapes in Fig.4.3a-b and 4.4a-b are bladelike and hexagonal types which could not be readily worn when the load is applied [36].

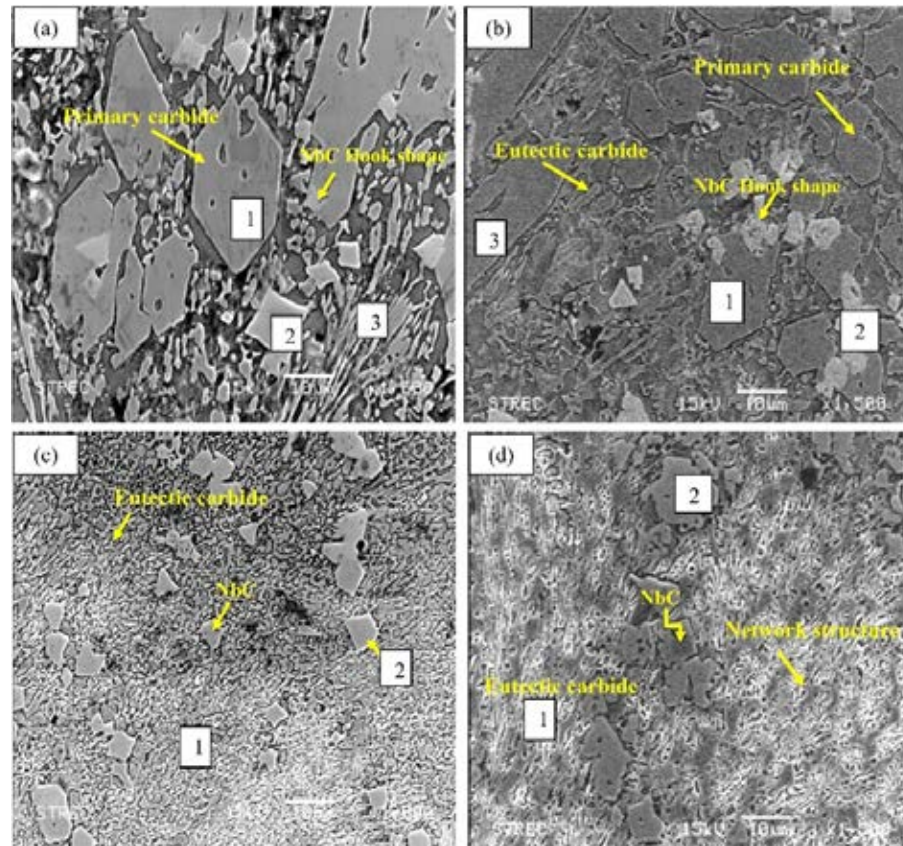


**Figure 4.4** Microstructure of the top surface of samples obtained by SEM (a) sample S1 (b) sample S2 (c) sample S3 (d) sample S4. The numbers are the EDX analytical positions for the results in Fig. 4.6

Since Gibbs free energy of formation of  $\text{Cr}_7\text{C}_3$  is more negative value than NbC and  $\text{Mo}_2\text{C}$  at any temperature [37]. Ternary equilibrium phase diagram of Fe-Cr-C is representative to discuss the microstructure after solidification.

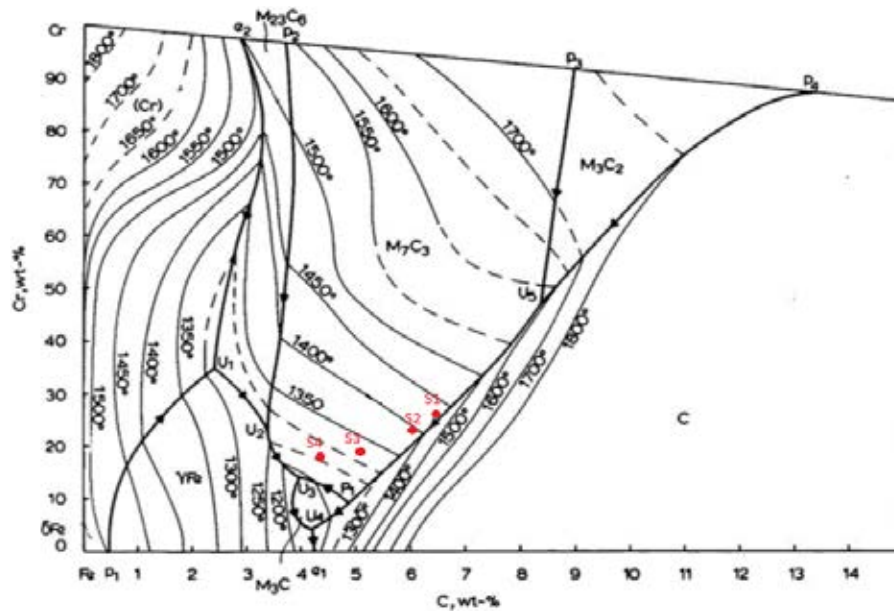


**Figure 4.5** Ternary phase diagram of Fe-Cr-C system [38]

Ternary phase diagram of Fe-Cr-C system (Fig.4.5) have reviewed by C.-M. Chang [38], and V.E. Buchanan [39]. However it can be calculated from Thermocalc software [40], during the solidification,  $M_7C_3$  are firstly precipitated by reaction ( $L \rightarrow L + M_7C_3$ ) called “Primary carbide” and the remained liquid is changed to eutectic carbide by the eutectic reaction ( $L \rightarrow fcc + M_7C_3$ ). After that fcc structure could be transformed to bcc structure during cooling process. In Fig.4.3a and 4.4a, the primary carbide should be the coarse particle. The observed fine carbides should be eutectic carbide. When Mo contents are 6.43 and 10.19 wt-%, the coarse carbide particles become smaller round carbide particles as shown in Fig.4.3c-d and 4.4c-d. This implies that Mo improve carbide distribution. During solidification Mo may accelerate eutectic reaction [14-15] as well as increase carbides nucleation sites. The network structure was seen in Fig. 1d when the Mo content is 10.19 wt-%.

For clear understanding in the observed microstructures shown in Fig.4.4, it should be simultaneously discussed with both EDX and XRD results. Fig.4.6a-d shows the EDX spectra corresponding to the analytical positions shown in Fig.4.4, respectively. Fig.4.7a-d shows the



EDX spectra of samples S1-S4. Table 4.2 summarizes the observed phases in samples S1-S4 from XRD patterns.

For sample S1 without Mo, the hexagonal and bladeliike coarse carbide, No.1 in Fig.4.4a, is contained of high chromium and iron contents as shown in EDX spectrum, No. 1 in Fig.4.6a. It is probably chromium-rich carbide,  $(Fe, Cr)_7C_3$  [11-12,42-43].

The rectangular and brighter particle, No.2 in Fig.4.4a, shows mainly Nb peak in the EDX spectrum, No.2 in Fig.4.6a. This carbide is rich in Nb. Therefore, it should be niobium carbide. This hook shape niobium carbide is embedded in  $(Fe, Cr)_7C_3$  as marked in Fig.4.4a and b. It hold  $(Fe, Cr)_7C_3$  from breaking by keeping  $(Fe, Cr)_7C_3$  intact resulting in improve abrasive wear resistance [44]. The EDX spectrum of fine carbide particle, No.3 in Fig.4.4a and 4.6a, shows the similar spectrum to the coarse carbide No.1. These fine carbides sit in between the coarse carbide. They could be the eutectic chromium-rich carbides coming from eutectic reaction during solidification [38-39]. The XRD spectrum of sample S1 in Fig.4.7a clearly show the peaks of  $(Fe, Cr)_7C_3$  and NbC particles. This means that coarse carbide at No.1 and fine carbide at No.3 in Fig.4.4a are the same  $(Fe, Cr)_7C_3$  carbide.

For sample S2 with 2.96%Mo, the EDX spectrum of hexagonal shape carbide at No. 1 in Figs.4.4b and 4.6b show the peak of Mo which is not found in the any position in sample S1, No.1 in Figs.4.4a and 4.6a. Molybdenum may be dissolve into the chromium-rich carbide,  $(Fe, Cr)_7C_3$ , to form mixed metal carbide,  $M_7C_3$  or  $(Fe, Cr, Mo)_7C_3$  which is shown in the XRD spectrum as shown in Fig.4.7b.

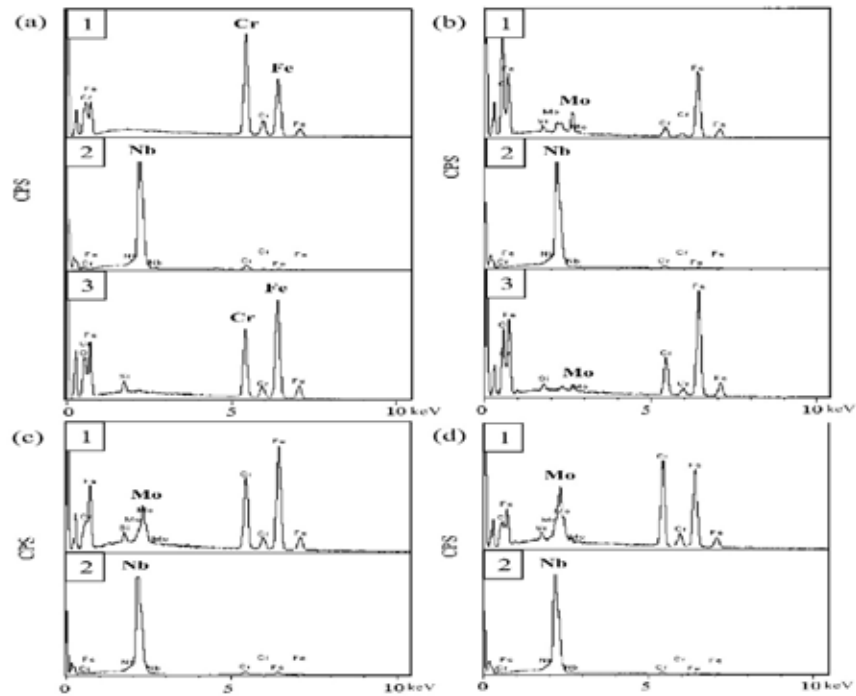


**Figure 4.6** EDX spectra of different position on the microstructure of samples (a) sample S1 (b) sample S2 (c) sample S3 (d) sample S4

In Fig.4.4b, the hexagonal shape carbide, No. 1, and the blade-like carbide, No.3, compose of similar pattern in the EDX spectra in Fig.4.6b, No.1 and 3. They should be the same carbide but different in orientations [45-47]. In the niobium rich carbide, No.2 in Figs.4.4b and 4.6b, the no Mo peak is found. Mo may not involve in the formation of niobium rich carbide. The NbC is also observed in XRD spectrum as in Fig.4.7b. NbC is embedded in  $(Fe, Cr, Mo)_7C_3$  as shown in Fig.4.4b same as sample S1. This could help  $(Fe, Cr, Mo)_7C_3$  to resist breaking. In addition, the XRD spectrum in Fig. 4.7b also show  $Mo_2C$  peak.

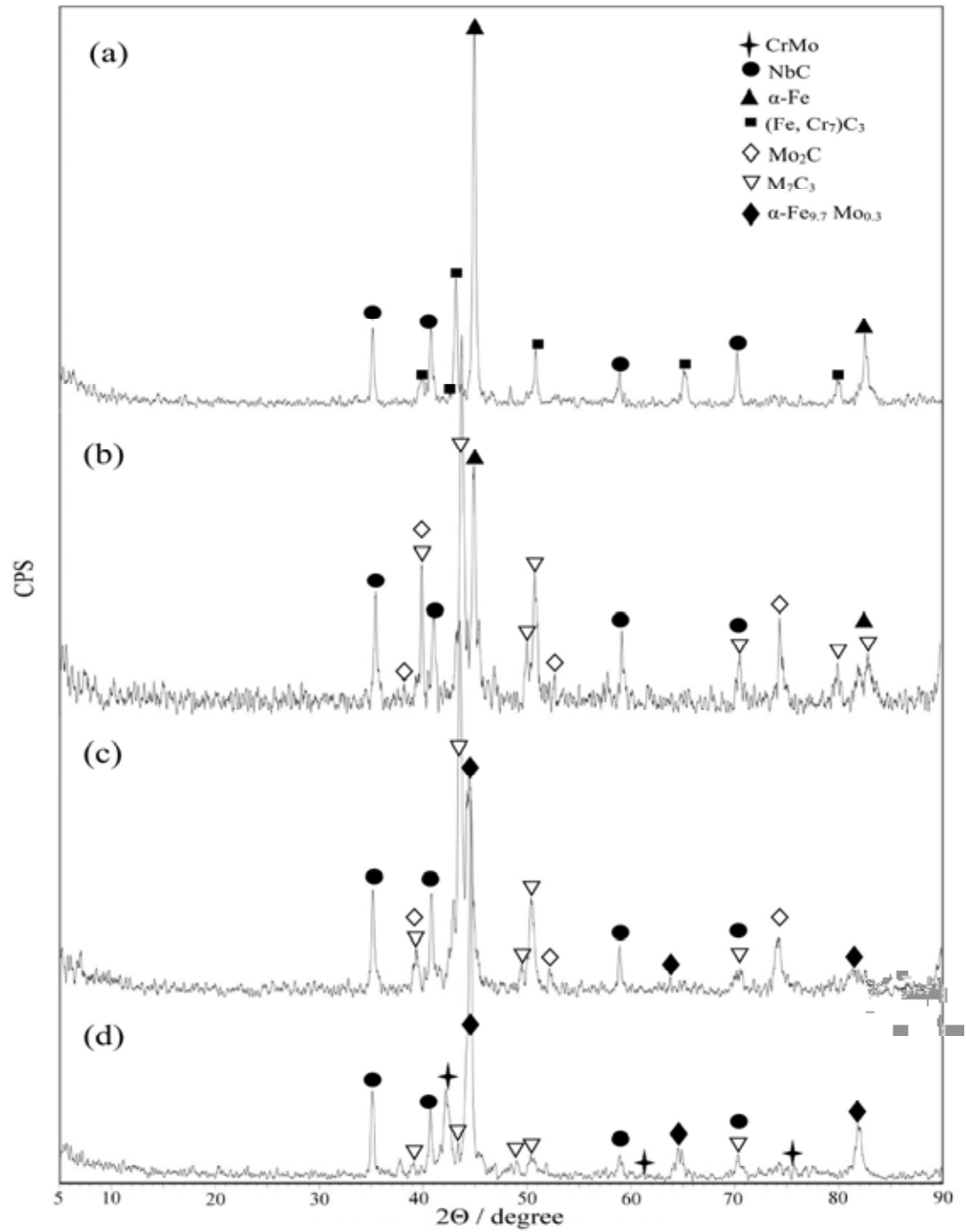


**Figure 4.7** XRD patterns of hardfacing samples (a) sample S1 (b) sample S2 (c) sample S3 (d)

sample S4

**Table 4.2** Phases for different samples from XRD patterns

Phase	Sample			
	S1	S2	S3	S4
CrMo				X
NbC	X	X	X	X
$\alpha$ -Fe	X	X		
(Fe, Cr) $_7$ C $_3$	X			
Mo $_2$ C		X	X	
M $_7$ C $_3$ or (Fe, Cr, Mo) $_7$ C $_3$		X	X	X
$\alpha$ -Fe $_{0.97}$ Mo $_{0.3}$			X	X

For sample S3 with the 6.43%Mo, the coarse M $_7$ C $_3$  carbides disappear but the fine carbides are found in Fig.4.4c. The EDX spectra of these fine carbides, No.1 in Fig.4.6c, are similar pattern to the coarse M $_7$ C $_3$  carbides, No.1 in Fig.4.6a and b. Molybdenum may increase carbide nucleation sites resulting in increasing volume fraction of small carbide [13-17]. Molybdenum dissolved into (Fe, Cr) $_7$ C $_3$  become (Fe, Cr, Mo) $_7$ C $_3$ , it give more negative value of enthalpy of mixing[48]. Rate of nucleation is a function of exponential of negative Gibbs free energy of formation [49] and Gibbs free energy of formation is function of enthalpy of mixing when Gibbs free energy comes more negative value so that more nucleation rate can be achieved. The XRD pattern of sample S3 as shown in Fig.4.7c also shows existing of Mo $_2$ C, NbC, and intermetallic  $\alpha$ -Fe $_{0.97}$ Mo $_{0.3}$ . The intermetallic  $\alpha$ -Fe $_{0.97}$ Mo $_{0.3}$  could possibly occur because of Mo saturation in M $_7$ C $_3$ . Dissolving of Mo in  $\alpha$ -Fe give solid solution effect.

Sample S4 with the Mo content of 10.19 wt-%, the network structure appears as shown in Fig.4.3 and 4.4d. The EDX and XRD results, Fig.4.6d and 4.7d, show also the presence of M $_7$ C $_3$ , Mo $_2$ C, NbC,  $\alpha$ -Fe $_{0.97}$ Mo $_{0.3}$ , except the CrMo phase. The presence of CrMo phase is possible according to their phase diagram [50], It is probably responsible for the network structure. The solidification mechanism may change when molybdenum content is more than 6.43 wt-%. The melting points of M $_7$ C $_3$  and CrMo are about 2,000 and 2,200°C, respectively [37,50]. It says that during solidification, the CrMo precipitates before M $_7$ C $_3$  and may accumulate at the grain boundary to form the network structure, which could cooperate with carbide or  $\alpha$ -

$\text{Fe}_{0.97}\text{Mo}_{0.3}$ . This should be further investigated. The EDX and XRD results of samples S3 and S4 confirm that Mo does not have any effect on NbC.

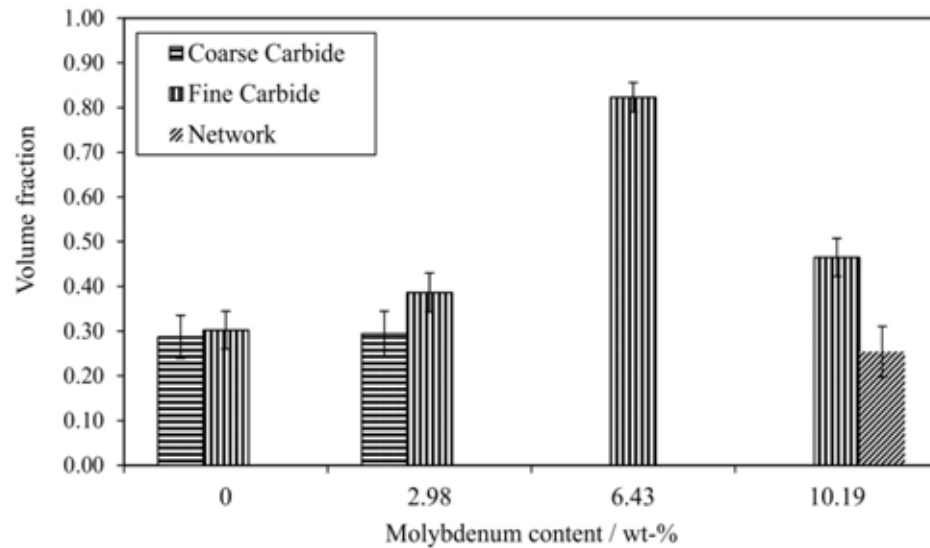


**Figure 4.8** Volume fraction of primary and eutectic carbides with respect to the molybdenum contents

Fig.4.8 shows volume fractions of coarse and fine carbides and network structure measured from microstructures observed by OM. The coarse carbide represents primary carbide for S1-S2. The fine carbide represents the eutectic carbide and small carbide particle which comes from the coarse primary carbide due to molybdenum effect. Coarse carbide fraction decreases but the fine carbide fraction increases when increasing molybdenum contents. The coarse primary carbide disappears and the fine carbide volume fraction reaches to the maximum content when molybdenum content is 6.43 wt-% (Sample S3). Because of these fine particles, sample S3 should perform the highest abrasive wear resistance. However, the volume fractions of fine carbide drops to 0.46 and the network structure appears with volume fraction of 0.25, when molybdenum content is 10.19 wt-%. This network structure may induce poor abrasive wear resistance. As discussed above, this network structure may involve with the CrMo phase.

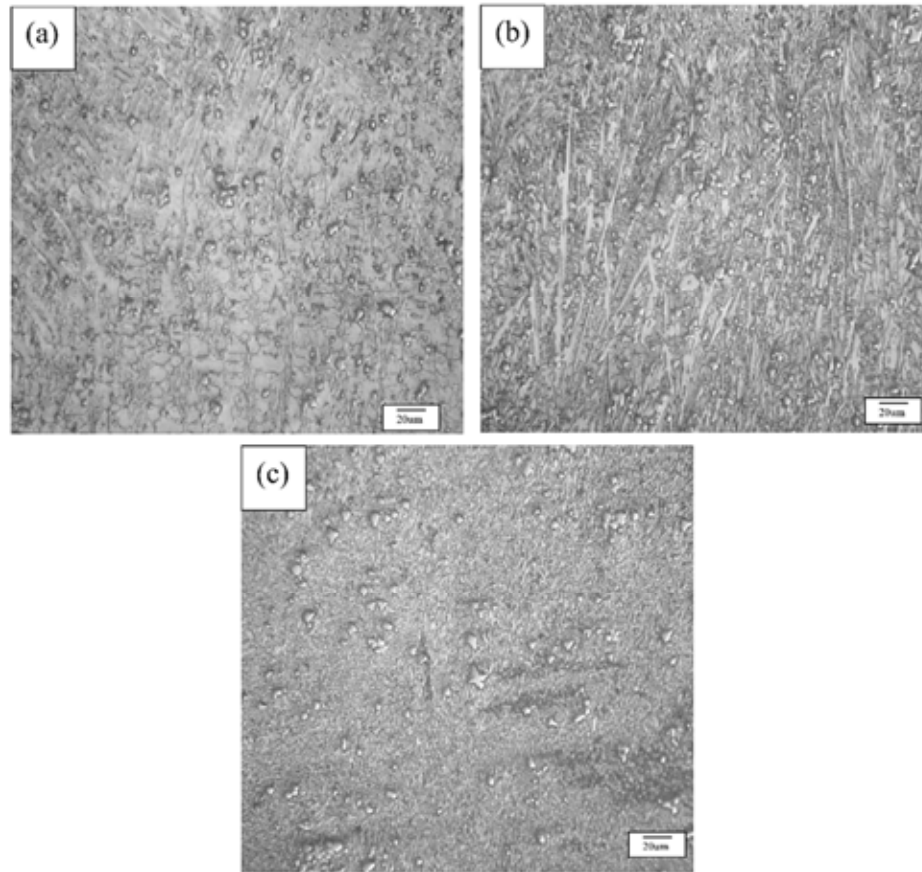


**Figure 4.9** Microstructure of different layer of sample S3 (a) first layer (b) second layer (c) third layer

For more understand about dilution that affected on microstructure. The microstructure of different sample S3 was observed. Fig.4.9 shows the cross-section microstructure of sample S3 in different layers. Fig.4.9a shows the first hardfacing layer of sample S3, which contains chromium carbide networks on matrix including NbC. The network of carbide is known to break very easily because it is brittle. However, in Fig.4.9b-c after applying the second and third hardfacing layer, fine primary and eutectic carbides are developed as well as carbide network disappeared because by applying more layers, it reduces dilution and influence of St52-3 steel including preheat from later layer.

Volume fractions of total carbides in each layer is shown in Fig.4.10. The trend of volume fractions of total carbides is higher when more layers are applied. The highest carbides volume fraction is in the third layer of surface. This means the highest abrasive wear resistance can be achieved on the third layer.

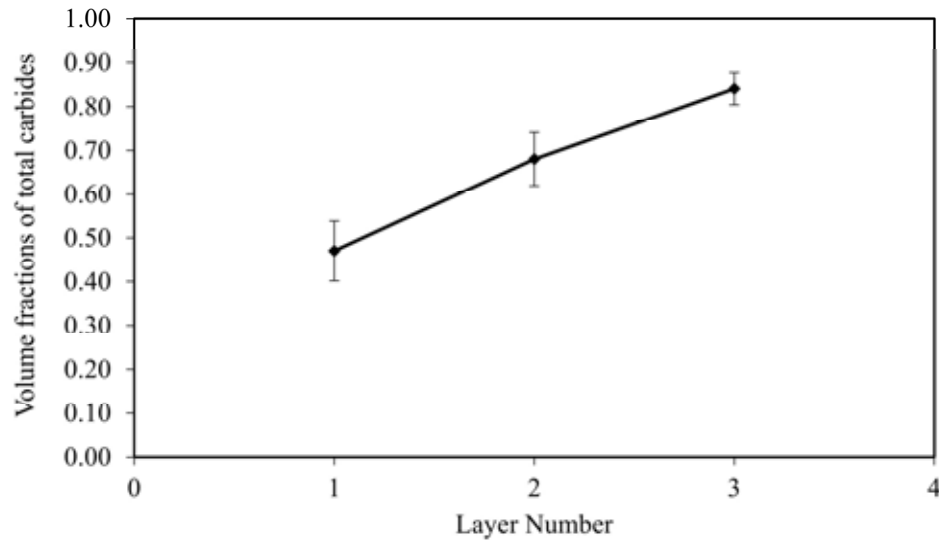


**Figure 4.10** Volume fraction of total carbides in each layer of sample S3

Fig.4.11 shows the distributions of Cr, Mo and Nb compositions along the distance from the base metal to the surface of sample S3 by using EPMA. The compositions of these three elements from the base metal to the surface increase because of less dilution in the surface layer as previously discussed. The high contents of chromium, niobium and Mo in third layer result in fine structure because of carbide distribution improvement. The evidence supporting microstructure is shown in Fig.4.9c.

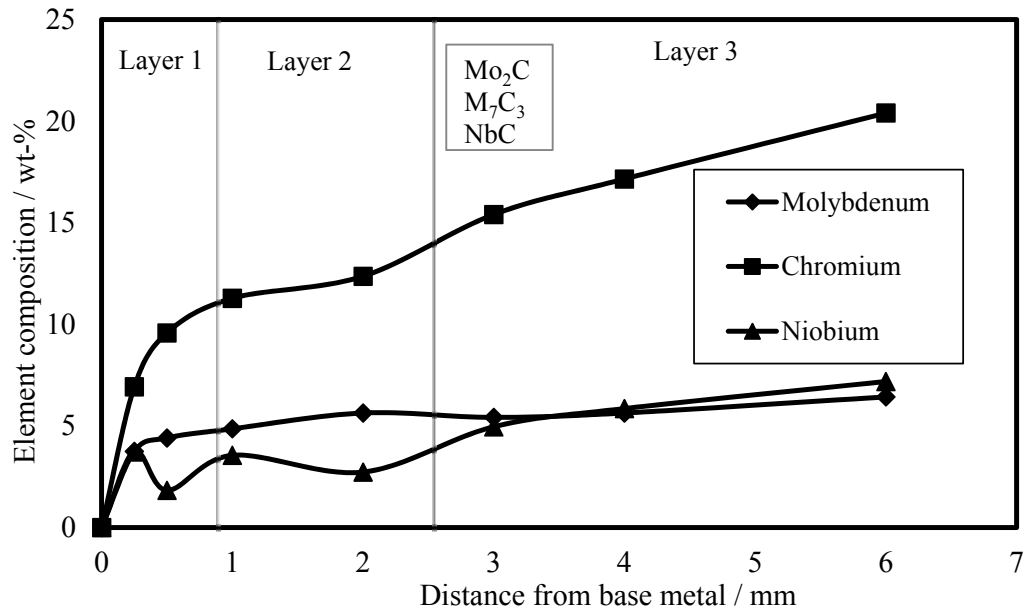


**Figure 4.11** Element composition in different layers of sample S3

#### 4.2 Microhardness and abrasive wear resistance

The microhardness and abrasive wear resistance of the top hardfaced surface of sample S1-S4 are showed in Fig.4.12. After wear test, volume loss was very small, thus the wheel diameter was insignificantly changed. In this work, the volume loss of St52-3 base metal is about  $110 \text{ mm}^3$ . The volume losses of hardfaced samples S1-S4 are less than  $5 \text{ mm}^3$ . This work reduces the volume loss of St52-3 steel by abrasive wear at least 95%.

The highest microhardness were found at Mo contents of 2.98 and 6.43 wt-%, corresponding to the hardfaced samples S2 and S3, respectively. The presence of  $\text{Mo}_2\text{C}$  in samples S2 and S3 may help to increase hardness. It was said that  $\text{Mo}_2\text{C}$  was usually formed at grain boundary [14-16], to retard grain deformation. However, the hardness decreases at Mo content of 10.19 wt-% (sample S4). This may be because of the presence of  $\alpha\text{-Fe}_{0.97}\text{Mo}_{0.3}$  and CrMo, which are softer than chromium carbide [51].



By wear test, the volume loss should also be the lowest at the highest microhardness. In this work, the abrasive wear resistance is the highest at the Mo content of 6.43 wt-% (sample S3). The volume fractions of carbide and carbide shape should be responsible for abrasive wear resistance of sample S2 and S3. Sample S3 has more volume fraction of fine carbide than sample S2. Hence, sample S3 performs higher abrasive wear resistance than sample S2. Sample S4 contains lower fine carbide volume fraction than sample S3.

The hardness of sample S4 is also lower than that of sample S3 because of the presence of the soft  $\alpha$ -Fe<sub>0.97</sub>Mo<sub>0.3</sub> and CrMo. From above reasons, the abrasive wear resistance of sample S4 is lower than that of sample S3.

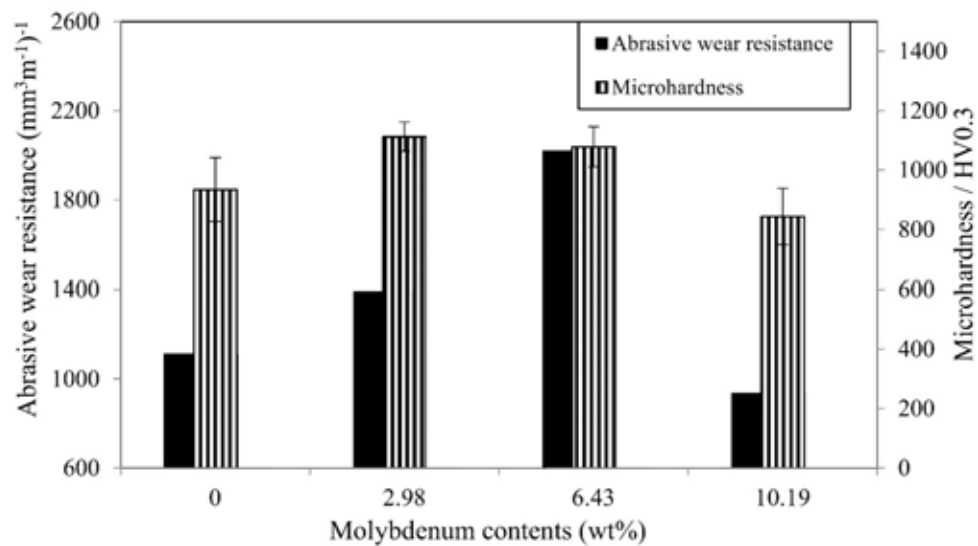


**Figure 4.12** Microhardness, volume loss and abrasive wear resistance of samples with different molybdenum contents

SEM image in Fig.4.4, samples S1 and S2 contain coarse and fine carbides and NbC. Sample S3 contains fine and hard carbide ( $M_7C_3$ ) as well as NbC. This fine  $M_7C_3$  may prevent NbC from easily breaking out. The smaller carbide gives more surface area to take the wear load and to bond with matrix compared with the larger carbide. Therefore, sample S3 performs better

wear resistance. In case of sample S4, the NbC, small carbide and network structure are present as in Fig.4.4d. The network structure may decrease abrasive wear resistance of sample S4.

Worn surfaces of all samples are present in Fig.4.13. In Fig.4.13a-c, it shows mostly microcutting and trail of missing carbides or pulling out of carbides from the hardfaced surface. This may occur after silica sand slide along the surface and destroyed brittle carbide. The extremely worn surface of hardfaced sample S4 is shown in Fig.4.13d.

In sample S4, it is also observed that porosity appears on the top surface of the sample. Silica sand may destroy area around porosity because very high stress concentrations can build up at porosity edge resulting in severe wear damage.

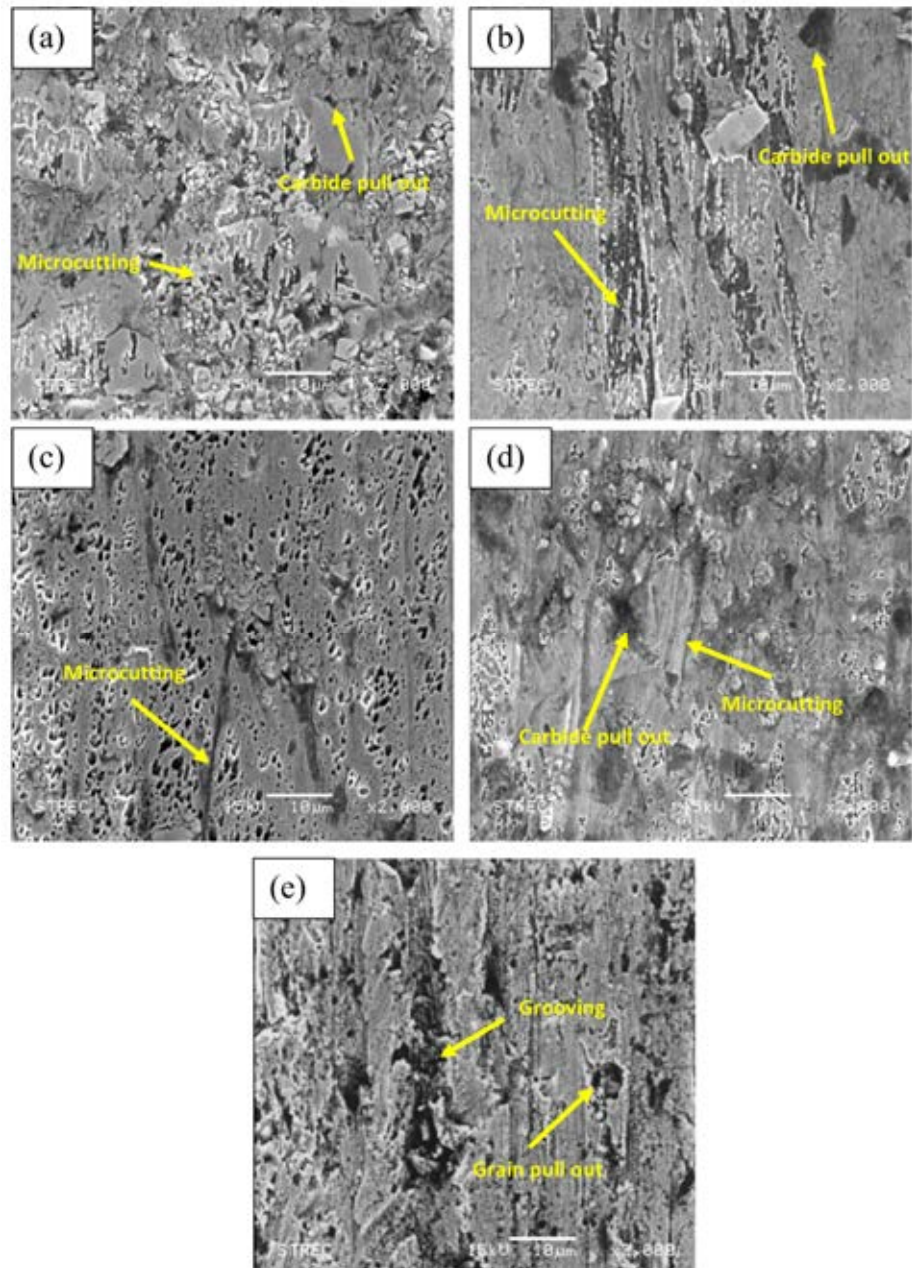


**Figure 4.13** Worn surfaces of (a) sample S1 (b) sample S2 (c) sample S3 (d) sample S4 (e)St52-3

## CHAPTER V

### CONCLUSION AND RECOMMENDATIONS

#### 5.1 General Conclusions

The conclusions can be summarized as follows:

1. The abrasive wear resistance of hardfacing St52-3 steel by SMAW is improved by using flux containing fixed Cr, Nb but different Mo contents coated on electrode.
2. Addition of molybdenum affects primary coarse  $(Fe, Cr)_7C_3$  carbide to form the smaller  $M_7C_3$  carbide by increasing the nucleation density during solidification, but does not affect on NbC formation.
3. The highest abrasive wear resistance of hardfacing St 52-3 steel is obtained when the molybdenum content in the hardfacing surface is 6.43 wt-% due to high hardness and high volume fraction of small carbide.
4. Main mechanisms of worn surface are microcutting and carbide pulling off.

#### 5.2 Recommendation

Both impact and abrasive wear of the hardfacing surface should be investigated at the same time, because very high speed shredder hammer hits the sugar cane by slightly impact and abrasive wear in the industrial condition. This means that special testing machine must be used for similarly industrial condition. However, this testing machine is not available in our laboratory.

## REFERENCES

- [1] Hugot, E., and Jenkins, G.H., Handbook of Cane Sugar Engineering, 3<sup>th</sup> edition, Amsterdam: Elsevier Science, 1986.
- [2] Zika Welding Electrode, Welding Catalog, Z-123 , Haifa, Israel, 2011.
- [3] Kirchgaßner, M., Badisch, E., and Franek, F., Behaviour of iron-based hardfacing alloys under abrasion and impact, *Wear*, 265 (2008): 772–779
- [4] S. Thongchitrusga, Shredder, Report 12/31/2010, Norton Interweld, Bangkok, Thailand, 2010.
- [5] Baligheid, R.G., Radhakrishna, A., Datta, A., and Rama Rao, V.V., Effect of molybdenum addition on structure and properties of high carbon Fe<sub>3</sub>Al based intermetallic alloy, *Material Science and Engineering*, A313 (2001): 117–122.
- [6] Hou, Q.Y., Influence of Molybdenum on the Microstructure and Properties of a FeCrBSi Alloy Coating Deposited by Plasma Transferred Arc Hardfacing, *Surface And Coating Technology*, 225 (2013): 11-20.
- [7] Mattar, A.R., and others, Influence of alloying elements Cu, Ni and Mo on mechanical properties and austemperability of austempered ductile iron, *International Heat Treatment and Surface Engineering*, 5 (2011): 78-82.
- [8] Li, W., Shan, S.F., and Fang, Q.H., Improvement of Ti–3Al–2V alloys by Mo reinforced alloying layer, *Surface Engineering*, 28 (2012): 594-597.
- [9] Chung, R.J., Tang, X., Li, D.Y., Hinckley, B., and Dolman, K., Microstructure refinement of hypereutectic high Cr cast irons using hard carbide-forming elements for improved wear resistance, *Wear*, 301 (2013): 695-706.
- [10] Wang, X.H., Han, F., Liu, X.M., Qu, S.Y., and Zou, Z.D., Effect of molybdenum on the microstructure and wear resistance of Fe-based hardfacing coatings, *Material Science and Engineering*, A489 (2008): 193–200.

- [11] Buchely, M.F., Gutierrez, J.C., Le'ón, L.M., and Toro, A., The Effect of microstructure on abrasive wear of hardfacing alloys, *Wear*, 259 (2005): 52–61.
- [12] Scandian, C., Boher, C., de Mello, J.D.B., and Rza-Aria, F., Effect of molybdenum and chromium contents in sliding wear of high-chromium white cast iron: The relationship between microstructure and wear, *Wear*, 267 (2009): 401–408.
- [13] Park, J.W., Lee, H.C., and Lee, S., Composition, microstructure, hardness, and wear properties of high-speed steel rolls, *Metallurgical and Material Transactions A*, 30A (1999): 399-409.
- [14] Hwang, K.C., Lee, S., and Lee, H.C., Effects of alloying elements on microstructure and fracture properties of cast high speed steel rolls Part I: Microstructural analysis, *Material Science and Engineering*, A254 (1998): 282–295.
- [15] Kim, C.K., and others, Effect of alloying elements on microstructure, hardness, and fracture toughness of centrifugally cast high-speed steel rolls, *Metallurgical Materials Transactions A*, (A36): 87–97.
- [16] M. Ikeda, and others, Effect of molybdenum addition on solidification structure, mechanical properties and wear resistivity of high chromium cast iron, *ISIJ International*, 32 (1992): 1157-1162.
- [17] Yao, M.X., Wu, J.B.C., and Xie, Y., Wear, corrosion and cracking resistance of some W- or Mo-containing Stellite hardfacing alloys, *Material Science and Engineering*, A407 (2005): 234–244.
- [18] Huang, J., Zhang, P.Z, Wu, H.Y., and Bao, W.J., Investigation of W-Mo alloyed layer synthesised by double glow plasma surface metallurgy, *Surface Engineering*, 27 (2011): 113-117.
- [19] Chang, X.T., and Sun, S.B., Effect of Mo on phase composition, microstructure and tribological property of TiC reinforced plasma sprayed coatings, *Surface Engineering*, 27 (2011): 300-305.

- [20] American Society of Testing and Materials, Test Method for Determining Volume Fraction by Systematic Manual Point Count, ASTM, E562 (2011):1-7.
- [21] American Society of Testing and Materials, Standard Test Method for Measuring Abrasion Using the Dry Sand/Rubber Wheel Apparatus, ASTM, G65 (2010): 1-12.
- [22] Shields, Jr. J.A., Applications of Mo metal and its alloys, International Molybdenum Association (1995): 2.
- [23] International Molybdenum Association, Molybdenum, London, BSC Print Ltd., 1998
- [24] Wikipedia, Molybdenum [Online]. 2011 Available from:  
<http://en.wikipedia.org/wiki/Molybdenum> [2011, November 12].
- [25] Bepari, M.M.A., and Shorowordi, K.M., Effects of molybdenum and nickel additions on the structure and properties of carburized and hardened low carbon steels, Journal of Materials Processing Technology, 155–156 (2004): 1972–1979
- [26] Zhang, X., Liu, N., and Rong, C., Effect of molybdenum content on the microstructure and mechanical properties of ultra-fine Ti(C, N) based cermets, Materials Characterization, 59 (2008): 1690–1696
- [27] Stackhowiak, G.W., and Batchelor, A.W., Engineering Tribology, 3<sup>rd</sup> edn., Oxford: Butterworth-Heinemann, 2005.
- [28] Connor, L.P., AWS Welding Handbook Volume I: Welding Technology, 8<sup>th</sup> edition, Miami, FL: American Welding Society, 1987.
- [29] Dr.-Ing. Winkler, International Welding Engineer, Berlin, Germany: SLV Duisburg, 2005.
- [30] O'Brien, R. L., AWS Welding Handbook Volume II: Welding Process, 8<sup>th</sup> edition, Miami, FL: American Welding Society 1987.
- [31] BOC.Limited, Industrial Product Reference Manual, New Zealand, BOC. Limited, 2006.
- [32] Callister, W. D., Jr., and Rethwisch D.G., Materials Science and Engineering: An Introduction, 7<sup>th</sup> edn, York, PA: John Wiley & Sons, 2010.

- [33] Davis, J.R., Alloying: Understanding the Basics, Materials Park, Ohio: ASM International 2001.
- [34] Jeshvaghani, R.A., Harati, E., and Shamanian, M., Effects of surface alloying on microstructure and wear behavior of ductile iron surface-modified with a nickel-based alloy using shielded metal arc welding, *Materials and Design*, 32 (2011): 1531–1536.
- [35] Egerton R.F., Physical Principles of Electron Microscopy, New York, NY: Springer Science, 2005.
- [36] Chang C., and others, Microstructure and wear characteristics of hypereutectic Fe–Cr–C cladding with various carbon contents, *Surface and Coating Technology*, 205 (2010): 245–250.
- [37] Barin, I., Thermochemical Data of Pure Substances, 3<sup>rd</sup> edn, Weinheim, VCH.: 1993.
- [38] Chang, C., ChunChen, Y., and Wu, W., Microstructural and abrasive characteristics of high carbon Fe–Cr–C hardfacing alloy, *Tribology International*, 43 (2010): 929–934.
- [39] Buchanan, V.E., Solidification and microstructural characterization of iron–chromium based hardfaced coatings deposited by SMAW and electric arc spraying, *Surface and Coating Technology* 203 (2009): 3638–3646.
- [40] Zhou, Y. F., and others, Wear resistance of hypereutectic Fe–Cr–C hardfacing coatings with in situ formed TiC, *Surface Engineer*, 29 (2013): 366-372.
- [41] Shin, J., Doh, J., Yoon, J., Lee, D., and Kim, J., Effect of molybdenum on the microstructure and wear resistance of cobalt-based Stellite hardfacing alloys, *Surface and Coating Technology*, 166 (2003): 117–126.
- [42] Qi, X., Jia, Z., Yang, Q., and Yang, Y., Effects of vanadium additive on structure property and tribological performance of high chromium cast iron hardfacing metal, *Surface and Coating Technology*, 205 (2011): 5510-5514.



- [43] Amirsadeghi, A., and Heydarzadeh Sohi, M., Comparison of the influence of molybdenum and chromium TIG surface alloying on the microstructure, hardness and wear resistance of ADI, Journal of Material Processing Technology, 201 (2008): 673-677.
- [44] Chen, H.X., and Chang, Z.C., Effect of niobium on wear resistance of 15%Cr white cast iron, Wear, 166 (1993): 197–201.
- [45] Coronado, J.J., Effect of  $(Fe, Cr)_7C_3$  carbide orientation on abrasion wear resistance and fracture toughness, Wear, 270 (2011): 287–293.
- [46] Kuo, C.W., Fan, C., Wu, S.H., and Wu, W., Microstructure and Wear Characteristics of Hypoeutectic, Eutectic and Hypereutectic  $(Cr, Fe)_{23}C_6$  Carbides in Hardfacing Alloys, Materials Transactions, 48 (2007): 2324-2328.
- [47] Dogan, O.N., and Hawk, J.A., Effect of carbide orientation on abrasion of high Cr white cast iron, Wear, 189 (1995): 136-142.
- [48] Wang Y.P., Li D.Y. , Parent L., and Tian H., Improving the wear resistance of white cast iron using a new concept – High-entropy microstructure, Wear, 271(2011): 1623-1628.
- [49] Porter D.A., Easterling K.E. and Sherif M.Y., Phase transformations in metals and alloys, 3<sup>rd</sup> edition, Florida: CRC press, 2009.
- [50] Qiu, C., Thermodynamic analysis and calculation of the Cr-Mo-C system, Journal of Alloys and Compounds, 199 (1993): 53-59.
- [51] Sheng, L.Y., and Guo, J.T., Microstructure and mechanical properties of NiAl–Cr(Mo)/Nb eutectic alloy prepared by injection-casting, Materials and Design, 30 (2009): 964–969.

## BIOGRAPHY

**Name-Surname** :Mr. Nut Thongchitrugsa

**Date of birth** :Monday 12<sup>th</sup> December 1988

**Address** :41 Soi Udomsuk7, Sukhumvit 103 Rd.,  
Bangna, Bangkok 10260

**Educational** :Primary School levels at Assumption Samutprakarn academic year 2544  
:Secondary School levels at Assumption Samutprakarn academic year 2547  
:Bachelor's degree in Mechanical Engineering  
Faculty of Engineering King Mongkut's University of Technology Thonburi  
academic year 2550  
:Master's degree in Metallurgical Engineering  
Faculty of Engineering Chulalongkorn University academic year 2554

**Email** : nutshogun@hotmail.com